universität wien

MASTERARBEIT / MASTER'S THESIS

Titel der Masterarbeit / Title of the Master's Thesis

„Specificities of human CD4+ T cell responses to the live attenuated yellow fever virus vaccine (17D-204)"

verfasst von / submitted by

Maximilian Koblischke, BSc

angestrebter akademischer Grad / in partial fulfilment of the requirements for the degree of

Master of Science (MSc)

Wien / Vienna, 2016

Studienkennzahl lt. Studienblatt / degree programme code as it appears on the student record sheet:	A 066 830
Studienrichtung lt. Studienblatt / degree programme as it appears on the student record sheet:	Masterstudium Molekulare Mikrobiologie, Mikrobielle Ökologie und Immunbiologie
Betreut von / Supervisor:	o. Univ. Prof. Mag. Dr. Franz X. Heinz

Acknowledgement

I want to sincerely thank Prof. Franz X. Heinz for giving me the opportunity to do my master´s thesis at the interface of virology and immunology and his scientific guidance.

I am thankful to Dr. Judith H. Aberle for the inspiring discussions regarding the scientific background of the project.

I want to thank Dr. Karin Stiasny for the scientific support concerning protein structures.

I am grateful to Ursula Sinzinger, Cornelia Stöckl and Jutta Hutecek for their support and expertise in laboratory tests.

I also want to thank all the other people from the Department of Virology for the pleasant working atmosphere and the fun we had outside the lab.

I am deeply grateful to my family and friends for the exceptional support during my studies.

Table of content

Abstract

Yellow fever virus (YFV) is a member of the genus flavivirus that includes several other important human pathogens such as dengue, West Nile or tick-borne encephalitis viruses which pose an increasing threat to humans worldwide. The live attenuated YFV vaccine (YF-17D) constitutes one of the most effective vaccines, inducing long-term protective immunity in almost all individuals. Neutralizing antibody responses, directed against the major envelope protein (E), are an established correlate of protection against flaviviruses. The effective production of such antibodies by B cells requires direct interaction with cognate CD4+ T cells which recognize MHC-II-restricted peptide epitopes derived from proteins, internalized by E-specific B cells through B cell receptor (BCR)-dependent uptake of virus particles. For flaviviruses, helper T cell epitopes cannot only be derived from E but also from the other structural proteins C (capsid) and prM/M (membrane).

The specificity of CD4+ T cell responses to viral proteins is usually restricted to a few immunodominant epitopes. The factors that determine immunodominance are still largely unknown but it has been suggested that in addition to peptide-MHC-II affinity, the three-dimensional (3D) protein structure can influence the endosomal selection of epitopes and shape the specificity of subsequent CD4+ T cell responses.

In the present study, we determined the overall extent and immunodominance patterns of human CD4+ T cell responses to YFV structural proteins C, prM/M and E in peripheral blood mononuclear cells (PBMCs) from 76 YF-17D vaccinees, using a highly sensitive interleukin-2 (IL-2) enzyme-linked immunosorbent spot (ELISPOT) assay and overlapping 15-mer peptides covering the entire sequence of each protein. The experimentally determined epitopes were analyzed in relation to the 3D structures of flavivirus C and E proteins as well as to *in silico* peptide-MHC-II affinity predictions.

The results of this study showed that the overall CD4+ T cell response was directed against all YFV structural proteins but predominately against the major envelope protein (E) and the capsid protein (C). Moreover, we identified eight immunodominant peptides which located to specific structural domains of C and E. The *in silico* predictions of peptide-MHC-II affinity revealed that the dominant epitopes in C were also the most frequently predicted peptides. However, for the E protein, immunodominant epitopes were not indicated by the prediction algorithm and the most frequently predicted epitopes were not identified experimentally.

This work provides new information on the CD4+ T cell specificity and immunodominance induced by the live attenuated YFV vaccine. Furthermore, our results indicate an influence of protein structural features on the selection of CD4+ T cell epitopes and on the reliable prediction of such epitopes by current computer algorithms.

Zusammenfassung

Das Gelbfieber Virus gehört zu der Gattung der Flaviviren, welche auch andere bedeutende Krankheitserreger wie Dengue, West Nil oder FSME Viren beinhaltet, die weltweit ein großes humanmedizinisches Problem darstellen. Der attenuierte Gelbfieber Lebendimpfstoff (YF-17D) ist eine der effektivsten Vakzinen und induziert einen Langzeit Schutz in fast allen Geimpften. Neutralisierende Antikörper gegen das Hüllprotein (E) sind ein Korrelat für den Schutz gegen Flaviviren. Diese Antikörper werden von B Zellen mit Hilfe von CD4+ T Zellen produziert, die Peptid Epitope aus Proteinen, nach deren Aufnahme und Prozessierung durch E-spezifische B Zellen, erkennen. Im Fall von Flaviviren können T Helfer Zell Epitope nicht nur vom E Protein sondern auch von den beiden anderen Strukturproteinen C (capsid) und prM/M (membrane) stammen.

Die Spezifität der CD4+ T Zell Antwort gegen Virusproteine ist auf wenige immunodominante Epitope beschränkt. Die Faktoren, welche diese Immunodominanz bestimmen, sind bisher nicht restlos geklärt. Jedoch könnte, neben der Peptid-MHC-II Affinität, die dreidimensionale (3D) Proteinstruktur für die Epitopselektion und die Spezifität der CD4+ T Zellen entscheidend sein.

In dieser Studie haben wir das Ausmaß und die Immunodominanz Muster der humanen CD4+ T Zell Antwort gegen die Gelbfieber Virus Strukturproteine C, prM/M und E in mononukleären Zellen des peripheren Blutes von 76 YF-17D Geimpften mittels eines hoch-sensitiven Interleukin-2 (IL-2) enzyme-linked immunosorbent spot (ELISPOT) Test und überlappenden, die gesamte Proteinsequenz umspannenden, 15-mer Peptiden untersucht. Die experimentell bestimmten Epitope wurden in Relation zur 3D Struktur der Flavivirus C und E Proteine und *in silico* Peptid-MHC-II Affinität Vorhersagen analysiert.

Die Resultate dieser Studie haben gezeigt, dass die Immunantwort der CD4+ T Zellen gegen alle Strukturproteine, hauptsächlich aber gegen die E und C Proteine, gerichtet ist. Es konnten acht immunodominante Peptide in spezifischen Strukturelementen der C und E Proteine identifiziert werden. Die Computervorhersage der Peptid-MHC-II Affinität konnte alle dominanten Epitope des C Proteins prognostizieren. Im Gegensatz dazu wurden die immunodominanten Epitope des E Proteins nicht vorhergesagt und es wurden viele Peptide prognostiziert, welche experimentell nicht identifiziert wurden.

Diese Arbeit zeigt neue Informationen über die Feinspezifität und Immunodominaz der durch die Gelbfieber Impfung induzierten CD4+ T Zell Antwort. Die Ergebnisse lassen vermuten, dass strukturelle Faktoren der Proteinantigene die Selektion von CD4+ T Zell Epitopen sowie die zuverlässige Vorhersage dieser Epitope durch Computer Algorithmen beeinflussen.

1. Introduction to the scientific background

1.1. Classification of flaviviruses

The genus flavivirus belongs to the family of *Flaviviridae* and comprises more than 70 RNA viruses which are transmitted to their vertebrate hosts by infected mosquitoes, ticks or have no known vectors. The most important human pathogens constitute yellow fever virus (YFV), dengue virus (DENV), Japanese encephalitis virus (JEV), West Nile virus (WNV), tick-borne encephalitis virus (TBEV) as well as the just recently emerging Zika virus. Flaviviruses comprise different serocomplexes which were defined by cross-neutralizing polyclonal antibody sera. These serocomplexes correlate with the degree of the envelope protein amino acid sequence similarity (Fig. 1.1). Within a serocomplex, amino acid identity is greater than 60% whereas flaviviruses of different serocomplexes share only about 40% identical amino acids (90, 111, 132).

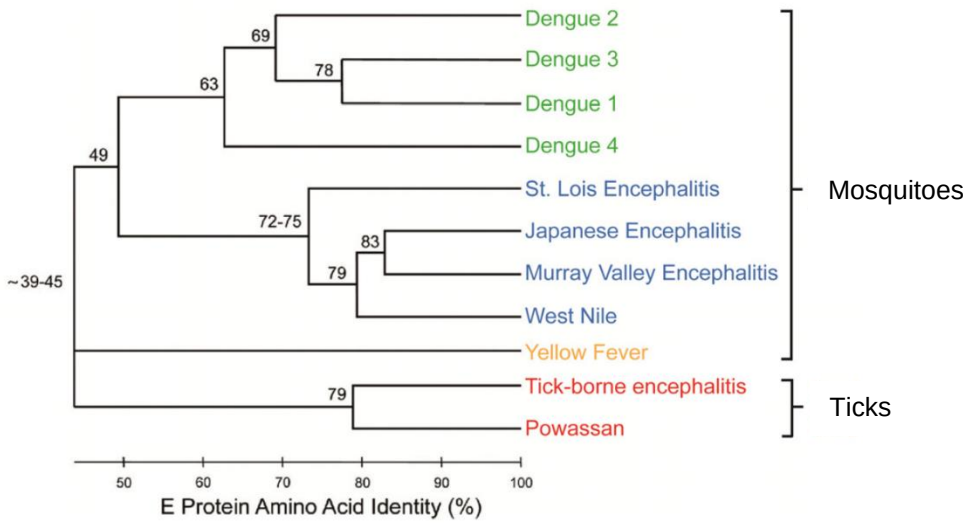

Fig.1.1 Dendrogram of flaviviruses. Relationship of different flaviviruses is mirrored by the E protein amino acid identity. Colors indicate serocomplexes of flaviviruses: dengue virus (green), Japanese encephalitis virus (blue), yellow fever virus (orange), tick-borne encephalitis virus (red). Transmission vectors are indicated in the right panel. Modified from (119).

1.2. Yellow fever virus

1.2.1. Epidemiology

Yellow fever virus (YFV) is endemic in the tropical and subtropical regions of Africa and America (Fig. 1.2.1). Two main transmission cycles have been reported. In the “sylvatic (jungle) cycle”, YFV is transmitted between mosquitos and populations of non-human primates. In the “urban transmission cycle”, the domestic *Aedes aegypti* constitutes the principal vector for YFV transmission between humans. In 44 affected countries, infection with YFV constitutes a serious public health threat for almost 900 million people. The WHO estimates 200,000 cases of yellow fever disease (30,000 deaths) each year (90% occurring in Africa) (42, 90).

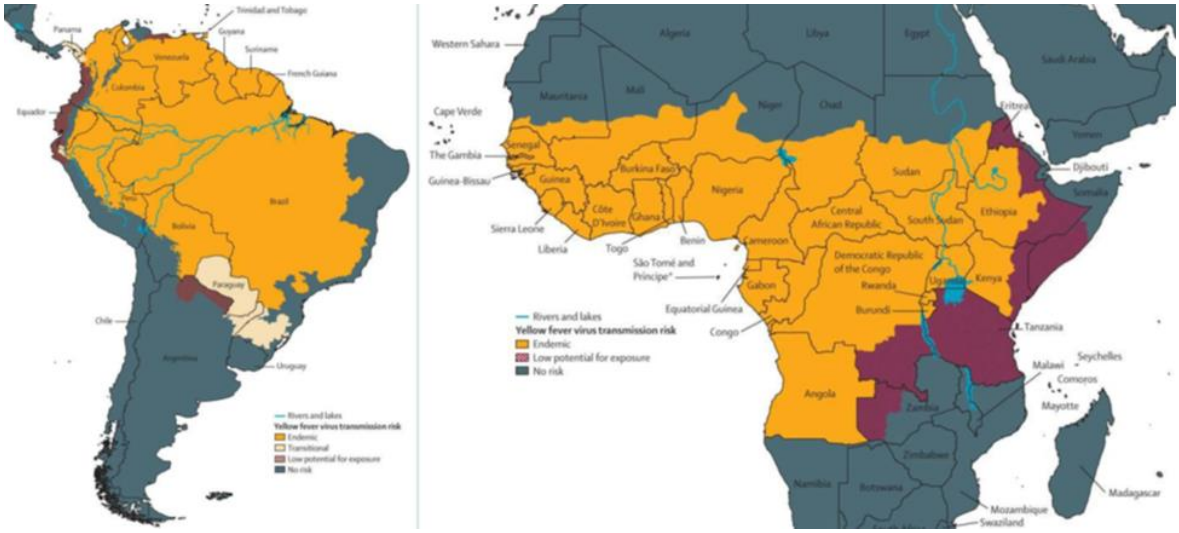

Fig.1.2.1 Areas with risk of YFV transmission in America and Africa. Areas colored in yellow indicate yellow fever virus endemic regions. Regions colored in magenta and dark grey exhibit low or no risk of virus transmission. Modified from (42).

1.2.2. Clinical signs and symptoms of YF

Severe yellow fever is characterized by high fever, hepatic failure, shock and 20-50% lethality. However, in most cases, YFV infection causes only mild symptoms (fatigue, headache, nausea and vomiting) and patients fully recover within a few days. There is no specific antiviral treatment available but the disease can be effectively prevented by a live attenuated virus vaccine (11, 73, 75, 90).

1.2.3. YF vaccination

The live attenuated YF virus vaccine (strain YFV-17D) has been developed in 1937. The parental Asibi strain was originally isolated from a Ghanaian patient with a mild febrile illness and subsequently passaged 176 times in embryonic mouse and chicken tissues until the YFV-17D strain was obtained. Two substrains (YFV 17DD and YFV 17D-204), derived from different passage numbers, are available as vaccines today (77, 90).

More than 500 million doses of YFV-17D have been administered (31, 131). One subcutaneous injection of yellow fever vaccine contains 10^4 to 10^6 plaque-forming units (PFU) and provides sustained immunity for 99% of vaccinees within 30 days (90, 131). According to the WHO, a booster dose is not necessary for protection (131). Serious adverse events (SAEs) have been reported at very low frequency (below 1 per 100,000 doses) (1, 56, 74, 90, 113). Vaccine-associated neurologic disease (YEL-AND) is characterized by viral invasion of the central nervous system. Patients with vaccine-associated viscerotropic disease (YEL-AVD) suffer from organ failures, similar to the symptoms following infection with wild type YFV.

1.3. Molecular biology of flaviviruses

1.3.1. Genome organization

The viral genome consists of a positive sense single stranded (ss) RNA molecule of approximately 11kB length. The genetic information is arranged in a single open reading frame (ORF) and translated into a polyprotein which is co- and post-translationally processed by host and viral proteases into three structural proteins: E (envelope), prM/M (precursor to membrane/membrane), C (capsid), and seven non-structural proteins: NS1, NS2A, NS2B, NS3, NS4A, NS4B and NS5 (Fig. 1.3.1) (55, 78).

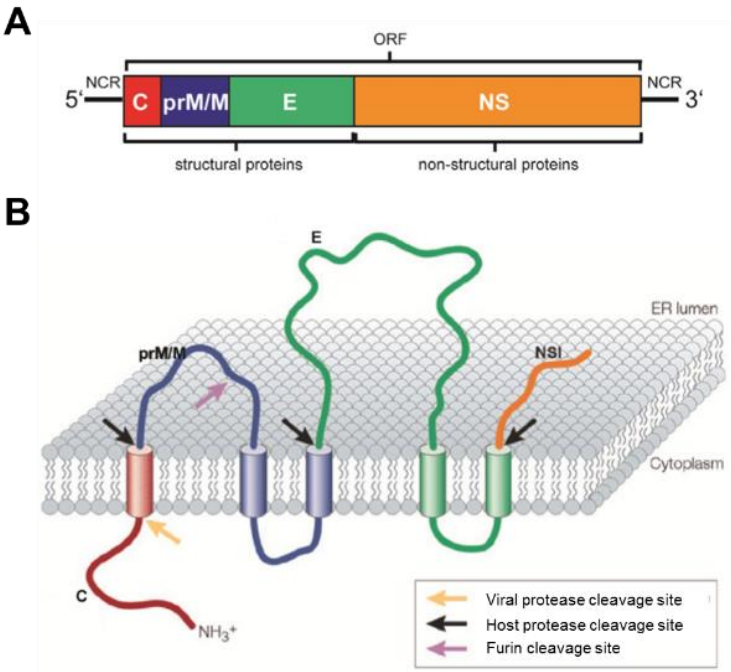

Fig. 1.3.1 Schematic representation of the flavivirus genome and the proteolytic processing of structural proteins. (A) The ssRNA genome comprises only one ORF which encodes 3 structural proteins (C, prM/M and E) as well as 7 non-structural proteins. The ORF is flanked by non-coding regions (NCRs). (B) Orientation of structural proteins in the endoplasmatic reticulum (ER). Processing sites of host and viral proteases as well as transmembrane domains of structural proteins are indicated by differentially colored arrows and cylinders, respectively. Modified from (78).

1.3.2. Virus particles

Immature viral particles are characterized by a diameter ~60nm and a spikey surface. Each of the 60 spikes is comprised of three prM-E heterodimers (Fig. 1.3.2 A and B, left panels). During virus maturation in the trans Golgi network (TGN), cleavage of prM results in the rearrangement of M-E heterodimers and the subsequent establishment of a smooth E protein shell in mature virions (Fig. 1.3.2 A and B, right panels) (48, 52, 55, 89).

Mature flavivirus particles are enveloped and spherical with a diameter of ~50nm. The virion comprises only three structural proteins (Fig. 1.3.2 A). The capsid protein (C) packages the genomic ssRNA. The major evelope protein (E) and the membrane protein (M) are anchored to a host-derived lipid membrane which surrounds the nucleocapsid. The envelope proteins do not exhibit physical contact to the capsid protein (55).

As determined by cryo-EM studies of dengue virus and West Nile virus, 180 copies of the two transmembrane proteins are present on the envelope of mature

virions (Fig. 1.3.2 B, right panel). The major envelope protein (E) occupies almost the entire virion surface. The smooth E protein shell of mature flaviviruses is composed of 90 homodimers which are orientated parallel to the lipid membrane and adopt a herringbone-like arrangement (30 rafts of three antiparallel E protein homodimers). The M protein resides underneath the E protein and is tightly associated with the membrane (55).

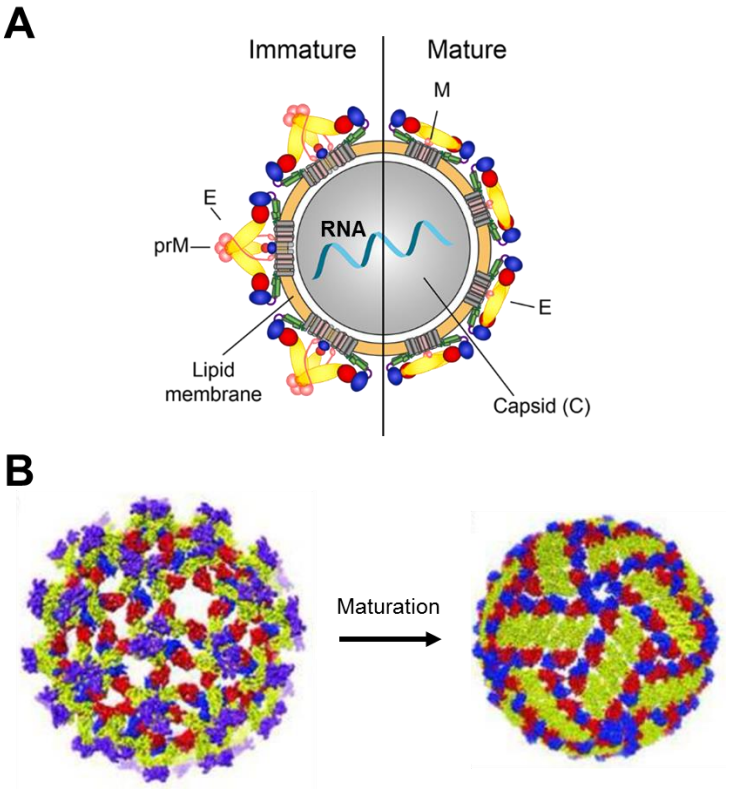

Fig. 1.3.2 Structural features of immature and mature flavivirus particles. (A) Schematic representation of the flavivirus particle. Flaviviruses contain one copy of the RNA genome as well as three structural proteins (C, prM/M and E). The envelope of immature virions (left panel) is characterized by spikes of prM-E heterodimers. During maturation, prM is cleaved into M. In mature virions, E proteins are arranged into homodimers that lie parallel to the virus membrane (right panel). (B) Pseudo-atomic structures of the surface of immature (left panel) and mature (right panel) flavivirus particles based on cryo-EM reconstructions. The surface of immature particles is characterized by 60 spikes, each formed by three prM-E heterodimers. The envelope of mature flaviviruses is characterized by a herringbone pattern which contains 30 rafts of three antiparallel E protein homodimers. Modified from (89).

1.3.3. Structural proteins

Capsid protein (C)

The highly basic capsid protein (C) has a molecular mass of ~11 kDa and does not contain disulphide brides or glycosylation motifs. Nuclear magnetic resonance (NMR) spectroscopy and X-ray crystallography analysis of Kunjin virus C protein revealed that capsid protein monomers contain four alpha helices and form dimers that are organized into tetramers (Fig. 1.3.3-1) (26). The hydrophobic alpha helix 2 is suggested to interact with the membrane and the positively charged alpha helix 4 with the RNA genome. For the N-terminus, no structural data is available (26, 45, 61).

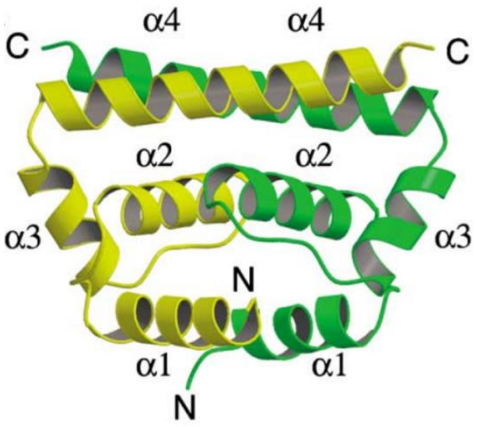

Fig. 1.3.3-1 Flavivirus capsid protein dimer. Ribbon representation of Kunjin virus capsid (C) protein dimer. Monomers (colored in yellow and green) associate in parallel orientation. Each C protein monomer comprises four alpha helices (α1-α4). Modified from (26).

Membrane protein (prM/M)

The precursor of the membrane protein (prM) is characterized by a molecular mass of ~26 kDa, 3 disulfide bonds and 1-3 glycosylation sites (55). The pr portion consists of 7 primarily anti-parallel beta strands, as shown by crystallographic data of dengue virus pr proteins (52). The membrane protein (M) has a molecular mass of ~8 kDa and comprises one ectodomain and two transmembrane domains (26, 90). For the M protein, no structural data is available.

Envelope protein (E)

The major envelope protein (E) has a molecular mass of ~53 kDa and can contain two glycosylation sites. Within the flavivirus envelope, the E protein ectodomain is connected to a double transmembrane (TM) anchor by a linker region termed stem (Fig. 1.3.3-2 A) (55, 134). Crystallographic analysis of soluble E proteins (lacking the TM and stem regions) from TBEV, DENV, WNV and JEV revealed a consistent three-domain (DI-DIII) architecture of the ectodomain (Fig. 1.3.3-2 C) (44, 59, 71, 72, 86, 94). Domain I (DI) is the central domain of the E protein. Eight beta sheets form a barrel structure that is stabilized by two disulphide bonds. Domain II (DII) projects from DI as a long finger-like domain, parallel to the virus surface. Three disulfide bridges stabilize an intertwined architecture of alpha helices, beta sheets and flexible coils. The tip of DII contains a short loop (the fusion peptide) which can interact with endosomal membranes as prerequisite for membrane fusion and nucleocapsid release. This sequence motif is highly conserved among flaviviruses (116). Domain III (DIII) protrudes from the opposite face of DI. The immunoglobulin-like fold is stabilized by one disulfide bond and consists of beta sheets and flexible coils. Evidence from WNV and DENV suggests that DIII might play a role in the engagement of cellular receptors during virus entry (23, 24, 100).

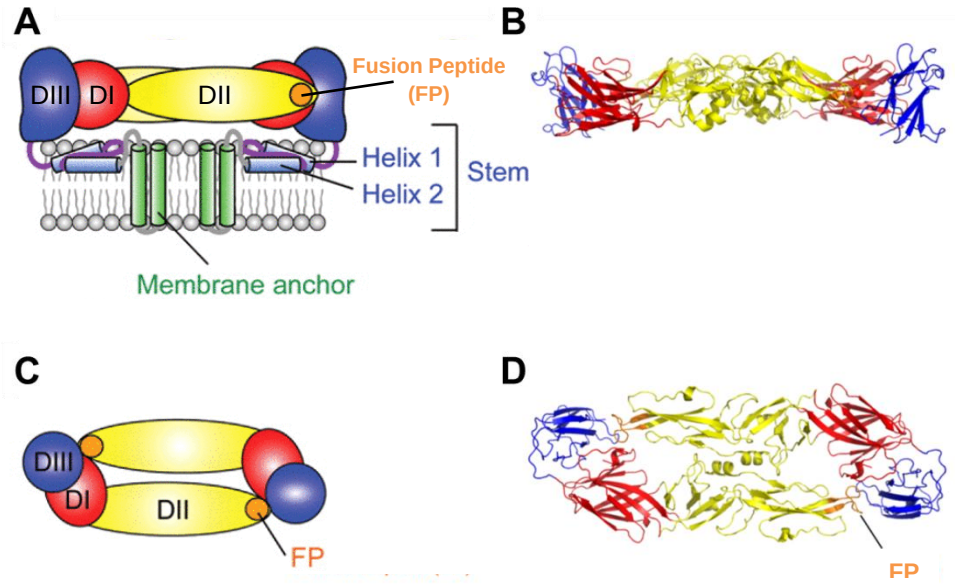

Fig. 1.3.3-2 Organization of E proteins on the surface of mature flavivirus particles. (A and B) Schematic and ribbon representation of the TBEV envelope (E) protein dimer (side view). Each E protein associates with the envelope through a double transmembrane (TM) anchor. The ectodomain comprises three domains (DI-DIII) and is linked to the TM domain by the stem region. Soluble E proteins used for crystallographic analysis lack the stem and anchor regions (B). (C and D) Schematic and ribbon representation of the TBEV E protein dimer (top view). Envelope protein monomers align in antiparallel orientation to form homodimers. Color codes of protein domains: DI (red), DII (yellow), DIII (blue), stem (purple/light blue) and TM (green). The fusion peptide (FP) on tip of DII is indicated in orange. Modified from (116).

During membrane fusion, the E protein shell undergoes dramatic rearrangements following exposure to pH<6.6 and envelope protein dimers of mature virions are reorganized to post-fusion E protein trimers (Fig. 1.3.3-3) (116, 118).

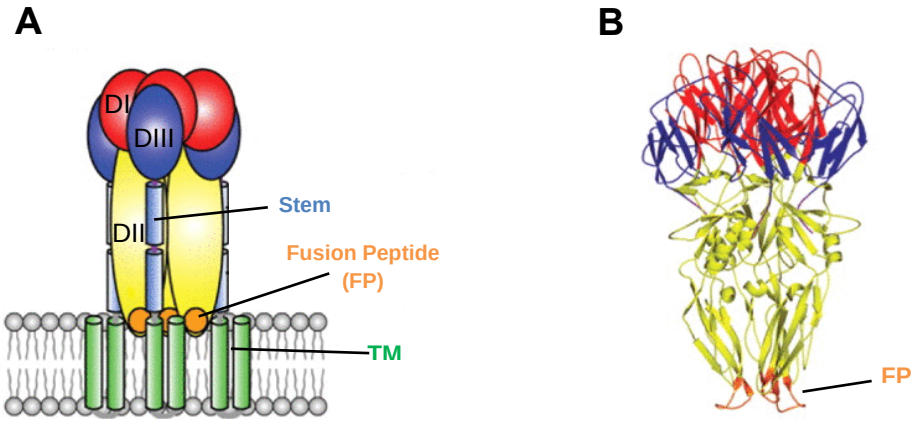

Fig. 1.3.3-3 Post-fusion structure of the E protein. (A) Schematic model of the TBEV post-fusion E protein trimer. Color codes: domain I (red), domain II (yellow), domain III (dark blue), stem (light blue) and transmembrane anchor (TM; green). The fusion peptide on the tip of domain II is indicated in orange. (B) Crystallographic structure of the TBEV sE protein lacking the stem and TM regions. Domains are colored as in (A). Modified from (116).

1.3.4. Life cycle

Attachment of flaviviruses to host cells is mediated by the interaction of flavivirus E proteins with cellular receptors (Fig. 1.3.4). Virus particles are then internalized through receptor-mediated endocytosis. Acidic pH in the endosome triggers structural rearrangements of E proteins which results in the insertion of the fusion peptide into the endosomal membrane and subsequently, the fusion of viral and endosomal membranes. By this process, the nucleocapsid is released into the cytosol, and the genomic ssRNA is uncoated, translated and replicated (90, 116, 118).

Immature virions are assembled by budding into the endoplasmatic reticulum (ER). In immature flavivirus particles, prM protein prevents the acid-induced rearrangement of E proteins, and thereby, premature membrane fusion. Accordingly, only after proteolytic processing of prM into M and pr proteins, mature infectious virus particles can be released. During exocytosis, immature viruses are subjected to the low pH of the trans-Golgi network (TGN) which exposes a furin cleavage site in prM. Following cleavage, the M portion remains anchored to the membrane of the viral envelope while the pr portion is lost from the virion after exposure to the neutral pH of extracellular space (78, 90).

However, virus maturation may be imperfect and can yield partially mature virions containing variable amounts of uncleaved prM (89). In fact, dengue virus infection produces a considerable proportion of partially mature virus particles which retain infectivity (43, 96, 99). In the case of flavivirus infection, also non-infectious capsid-less virus-like particles (VLPs) are formed which contain the E and M proteins but lack the nucleocapsid (37). The NS1 protein constitutes the only non-structural protein that is secreted from infected cells (37, 116).

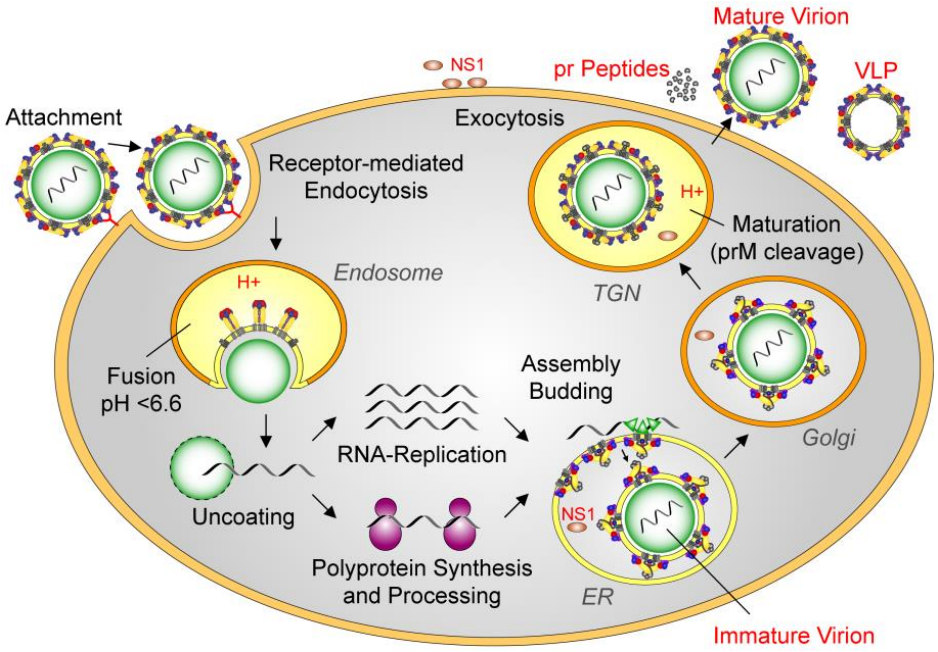

Fig. 1.3.4 Graphical summary of flavivirus life cycle. Receptor-mediated endocytosis of virus particles is followed by low pH-triggered endosomal fusion. The nucleocapsid is released into the cytoplasm and the ssRNA genome is uncoated. Genome translation and replication as well as assembly and budding of immature virus particles takes place at the membrane of the ER. Virions are subsequently exocytosed and acquire mature architecture following cleavage of the prM protein in the TGN. The pr portion is lost upon exposure to the neutral pH of the extracellular space. Modified from (116).

1.4. Immunity to flaviviruses

Cellular and humoral responses of the adaptive immune system play a critical role in virus clearance and long-term protection against flaviviruses (6, 12, 18, 36, 63, 66, 76, 112).

1.4.1. Humoral immunity

Antibody responses are crucial for protection against flaviviruses (36, 63, 76). The E protein is the major target for neutralizing antibodies because it occupies almost the entire virion surface and mediates important functions such as cell attachment or virus entry into host cells (91). The YFV-17D infection stimulates neutralizing antibody responses in virtually 100% of individuals within 30 days (13, 50, 88). Such antibodies have been found in human subjects, even decades after vaccination (92, 101). Moreover, experiments with non-human primates directly correlated the presence of neutralizing antibodies with protection from lethal challenge with YFV Asibi strain (63). For flaviviruses also detrimental antibody responses have been described. Antibody-dependent enhancement (ADE) of infection is likely enabled through poorly neutralizing antibodies which facilitate virus attachment to Fc receptors and the subsequent endocytosis of infectious virions into Fc receptor bearing cells. In patients, ADE was described after secondary DENV infection with a different serotype (91).

1.4.2. T cell help to B cells producing E-specific neutralizing antibodies

High affinity antibody responses are dependent on direct interactions between B cells and cognate CD4+ T cells. Cytokines and costimulatory molecules provided by CD4+ T helper cells facilitate the activation of B cells and induces proliferation, germinal centre formation, antibody isotype switching/affinity maturation as well as the generation of memory B cells (35, 125). The direct interaction requires that antigen-specific B cells internalize protein antigens through B cell receptor-mediated endocytosis and present processed peptides in complex with major histocompatibility complex class-II (MHC-II) molecules to the T cell receptor (TCR) of CD4+ T cells (2, 16, 29, 65, 102, 105, 106). In the case of B cells producing flavivirus-neutralizing antibodies, T helper cell epitopes can be derived not only from the envelope protein but also from the other two structural proteins (capsid and membrane) that are co-internalized as part of the viral particle by envelope-specific B cells (40, 62, 97, 107).

T cell help to E-specific B cells producing neutralizing antibodies is therefore restricted to CD4+ T cells specific for epitopes derived from the three structural proteins.

1.4.3. The CD4+ T helper cell responses to flavivirus structural proteins

The CD4+ T cell responses to flavivirus structural proteins are important for the production of neutralizing antibodies by E-specific B cells. With each of the structural proteins, only a few peptides are selected that dominate flavivirus-specific CD4+ T cell responses in mice (18, 25, 62, 124) and humans (40, 97, 107). In TBEV, it was shown that all three structural proteins C, prM/M and E contribute to the CD4+ T cell response (107). Immunodominant epitopes were located in helix two and four of the C protein. In the E protein, dominant epitopes were identified in all three domains. The immunodominant peptides of the TBEV E protein were exclusively located at the accessible protein surface (107). Moreover, in previous studies with HIV and influenza, CD4+ T cell epitope clusters were identified at exposed protein surfaces or at flanks of protease sensitive loops (49, 53, 69, 70, 81). Restriction to limited structural motifs of complex protein antigens indicates that features of the three-dimensional protein structure influence the selection of dominant CD4+ T cell epitopes.

1.5. Factors that influence the specificities of CD4+ T cell responses

1.5.1. MHC-II pathway

CD4+ T cells recognize short linear peptides in complex with major histocompatibility complex class-II (MHC-II) molecules on the surface of antigen presenting cells (APCs) such as dendritic cells (DCs) or B cells (2, 4). Endocytosed protein antigens or whole virus particles pass early and late endosomal compartments until they are finally degraded in the lysosome (Fig. 1.5.1) (16, 98). These compartments are characterized by an acidic pH and contain enzymes such as gamma-interferon-inducible lysosomal thiol reductase (GILT) or cathepsins to enable the breakdown of proteins. Endosomal proteases exhibit a broad substrate specificity and cleavage sites are mainly determined by their accessibility in the protein structure (15).

The MHC-II molecules are assembled in the endoplasmatic reticulum (ER) and comprise one alpha and one beta chain (Fig. 1.5.1) (16, 98). In the ER, MHC-II molecules associate with the invariant chain (Ii) which blocks premature peptide

binding and contains signal sequences to direct the MHC-II via the Golgi to endosomes/lysosomes. Subsequently, Ii is cleaved and a short fragment termed class-II-associated invariant chain peptide (CLIP) remains bound to the peptide binding cleft of the MHC-II molecule. The CLIP is eliminated from the peptide-binding MHC-II molecule after interaction with an accessory MHC-II molecule (HLA-DM). Subsequently, MHC-II molecules undergo conformational changes which facilitate CLIP dissociation and binding of high-affinity peptides (80, 93, 103). HLA-DM function is regulated by the accessory MHC-II molecule HLA-DO. The physiologic relevance of HLA-DO remains enigmatic but mechanistically, HLA-DO seems to act as a substrate mimic to prevent HLA-DM interaction with peptide binding MHC-II molecules (34, 64, 133).

In addition to this classical model of peptide loading onto MHC-II molecules, previous studies suggested a MHC-II guided antigen processing model. Here, rather large antigen fragments bind to the MHC-II molecule and are then trimmed to the final size (46, 98, 108). Moreover, recent reports indicated that also endogenous proteins can be substrates in the MHC-II pathway. Autophagic mechanisms or the transporter associated with antigen processing (TAP) may deliver antigenic substrates from the cytoplasm to endosomal compartments involved in MHC-II-restricted antigen processing (16, 28, 114). In fact, endogenously produced influenza proteins were identified as relevant source for CD4+ T cell epitopes (67).

Although numerous peptides of a complex protein antigen can be presented by MHC-II molecules, CD4+ T cell responses are usually restricted to a limited set of peptide epitopes. Several factors have been proposed to influence the specificity of an emerging CD4+ T cell response (47) including peptide-MHC-II affinity (51, 103), structural aspects of complex protein antigens (49, 53, 68, 70) and the frequency of specific T cells prior to virus exposure (41, 121).

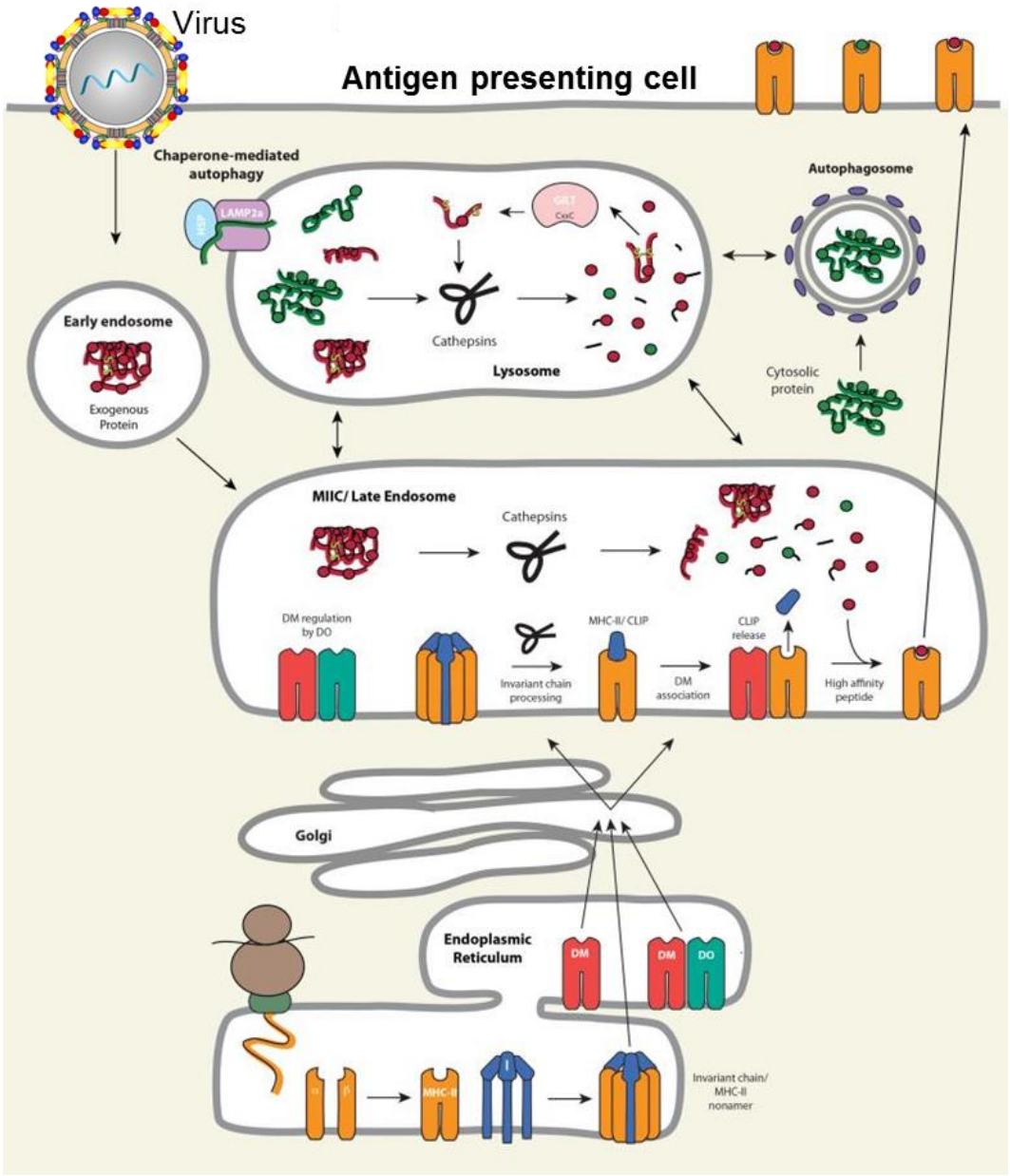

Fig. 1.5.1 Processing and loading of MHC-II-restricted peptide epitopes. The MHC-II pathway is responsible for the processing and presentation of protein antigens from exogenous and endogenous sources. The MHC-II molecule (orange) is constructed of an alpha and beta chain, and assembled in the ER together with the invariant chain (Ii) highlighted in blue. The Ii-MHC-II complex is transported to endosomal compartments via the Golgi. After cleavage of Ii, a short fragment termed CLIP remains bound to the peptide binding groove. The dissociation of CLIP and subsequent binding of high-affinity peptides is facilitated by HLA-DM (red). The action of HLA-DM is regulated by a second accessory MHC-II molecule (HLA-DO) indicated in cyan. Modified from (16).

1.5.2. Peptide-MHC-II affinity

The affinity of peptide-MHC-II complexes generated during antigen processing is an important factor that influences CD4+ T cell epitope specificities (104, 129). Such ligands are presented on the surface of antigen presenting cells (APCs) with dramatically increased half-lives ($t_{1/2}$ >150hrs) compared to low-affinity peptide-MHC-II complexes ($t_{1/2}$ ~10hrs) (51). Thus, high-affinity peptide-MHC-II complexes are more likely encountered by the TCR of CD4+ T cells than low-affinity complexes.

MHC-II molecules

Peptide-binding MHC-II molecules are heterodimers, consisting of non-covalently linked alpha and beta chains, each approximately 30 kDa large (Fig. 1.5.2). The N-termini form an extracellular peptide-binding cleft that is open at both ends and binds 10-30 amino acids long peptides. Binding of peptides is mediated by interactions between the peptide backbone and the edge of the cleft as well as by interaction between specific anchor residues and pockets within the floor of the MHC-II molecule (3, 10).

Human MHC-II molecules are co-dominantly expressed and encoded on chromosome 6 by three gene loci called human leukocyte antigen (HLA)-DP, HLA-DQ and HLA-DR. Alpha (HLA-XA) and beta (HLA-XB) chains of one individual are encoded by seven to eight genes (HLA-DPA1, -DPB1, -DQA1, -DQA2, -DQB1, -DRA1, -DRB1 and DRB3-5 which is not present in all human individuals). In addition, peptide binding MHC-II molecules are highly polymorphic with over 2600 distinct protein chains determined so far (27). Amino acid polymorphisms are primarily located to the peptide-binding groove of the beta chain (Fig. 1.5.2 B) and especially the HLA-DRB1 chain is highly polymorphic (>1400 distinct proteins). The HLA haplotype is defined as the set of alleles present on each chromosome. Thus, each heterozygous individual has two HLA haplotypes (3).

The diverse MHC-II molecules can have distinct peptide binding affinities and the cumulative binding preferences present within the human population are hypothesized to enable the presentation of any given peptide (3). However, different HLA alleles can have similar peptide binding preferences and these were clustered in HLA supertypes accordingly (33). The almost non-polymorphic accessory HLA molecules HLA-DM and HLA-DO are encoded in the same region of chromosome 6 and exhibit a similar structure but lack an accessible peptide binding groove (3).

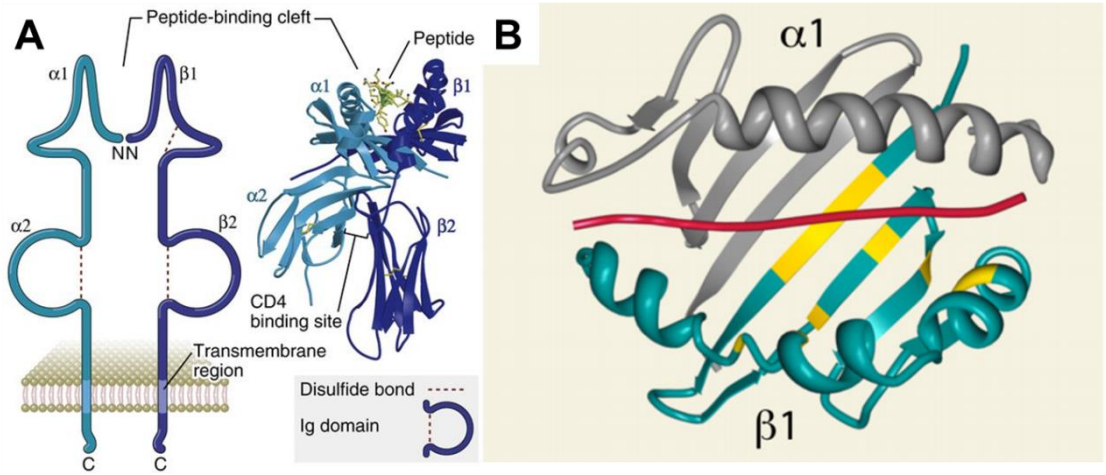

Fig. 1.5.2 Structural features of the MHC-II molecule. (A) Side view of the MHC-II molecule in schematic and ribbon representation (HLA-DR1 with influenza HA peptide). One alpha (cyan) and beta (blue) chain establish the MHC-II heterodimer. N-termini of both chains contribute to the formation of the peptide binding cleft, which is followed by Ig-like and transmembrane domains as well as a short cytoplasmatic tail on the C-terminus. The Ig-like domains harbor binding sites for the CD4 receptor on T cells. (B) Ribbon representation of the HLA-DR1 peptide binding groove with a bound peptide indicated in red (top view). The edge and floor of the cleft are established by two alpha helices and eight beta strands, respectively. Highly polymorphic residues within the beta chain are indicated in yellow. Modified from (3, 16).

Computer prediction of peptide-MHC-II affinity

In silico MHC-II binding predictions are often used for the pre-identification of CD4+ T cell epitopes (130). The majority of available algorithms use biochemical properties of the peptide sequence for prediction of binding to a given MHC molecule (82, 84, 85, 110, 120, 127, 128).

The Immune Epitope Database (IEDB) offers different algorithms such as Consensus, NetMHCIIpan or NN-align for the prediction CD4+ T cell epitopes (39). In the consensus approach, a binding score is calculated for peptide MHC-II complexes using different algorithms. The binding scores are compared against five million random peptides and subsequently a median percentile rank of the employed methods is generated. The IEDB suggests the predicted top 10% binding peptides of a protein antigen as likely MHC-II binders. Such evaluation is advantageous to the prediction of half maximal inhibitory concentration (IC_{50}) values if the peptide binding to different MHC-II alleles needs to be compared.

Epitope prediction algorithms are trained on large data sets of experimental peptide binding data. However, such experimental data is scarce for certain HLA

alleles and thus, training might be inefficient in some instances. Furthermore, current programs do not consider the peptide accessibility for MHC-II molecules during antigen processing, DM-mediated editing of the peptide repertoire or TCR binding (21, 54, 83). Studies with a variety of viral protein antigens, including TBEV, have shown that peptide-MHC-II affinity is not an accurate predictor of immunodominance *in vivo* and that only a fraction of peptides which can bind MHC-II molecules efficiently elicit dominant CD4+ T cell responses (8, 32, 95, 107).

1.5.3. Structural features of protein antigens

Several reports indicate that antigen structure may influence the selection of CD4+ T cell epitopes and thus, can modulate the specificity and epitope dominance of CD4+ T cell responses. Studies with a number of protein antigens have shown that epitopes which are not exposed at the surface of the native protein can be made accessible by immunization with denatured protein (109), antigen-derived peptides (103) or disulfide bond deletion mutants (53, 81). For example, immunization of mice with WT and disulfide-deleted variants of HIV gp120 revealed that high-affinity peptides deeply concealed within the three-dimensional protein structure may remain cryptic in WT protein but become functional CD4+ T cell epitopes in locally disordered disulfide mutants (53).

Furthermore, studies with HIV, influenza and TBEV revealed that dominant epitopes are located at exposed protein surface or at flanks of protease-sensitive loops (19, 49, 107, 122), supporting the notion that accessibility to proteolytic processing and MHC-II binding is an important determinant for epitope dominance in these proteins.

In addition, viral envelope proteins that undergo substantial conformational changes upon exposure to the acidic pH of the endosome, have the potential to expose immunogenic sites that may not be accessible in their native conformation on the surface of infectious virions, as has been shown for influenza hemagglutinin (22, 28). Together, these findings suggest that structural features and their pH-induced conformational changes can influence epitope presentation and CD4+ T cell specificities.

2. Objectives

The mosquito-borne yellow fever virus (YFV) constitutes a serious public health threat in the tropical and subtropical regions of Africa and America but yellow fever can be effectively prevented by a live attenuated virus vaccine (strain YFV-17D). Long-term protection against flaviviruses depends on the production of neutralizing antibody responses, directed against the major envelope protein (E). The production of such antibodies by B cells requires interaction with cognate CD4+ T cells which recognize MHC class-II-restricted peptide epitopes all of which are derived from protein antigens internalized by specific B cells. For flavivirus neutralizing antibodies, such T helper cell epitopes can not only be derived from the E protein but also from the other two structural proteins C (capsid) and prM/M (membrane) which are co-internalized with virus particles by E-specific B cells. The CD4+ T cell responses to viral pathogens are usually restricted to few epitopes. So far, the specific protein sites in YFV structural proteins that induce human T helper cell responses have not been determined.

The main objective of this master thesis is to determine the CD4+ T cell epitope specificities to the three YFV structural proteins in human PBMCs obtained from YF-vaccinated individuals. The CD4+ T cell epitopes will be identified in enzyme-linked immunosorbent spot (ELISPOT) assays after stimulation of CD8-depleted PBMCs using peptides that cover the entire amino acid sequence of C, prM/M and E. The experimentally identified epitopes will be analysed in the context of the three-dimensional structures of C, prM/M and E using available flavivirus protein crystal structures. Furthermore, we will determine the HLA alleles of YFV-17D vaccinees and analyse the experimental CD4+ T cell epitope data in relation to *in silico* MHC class-II epitope predictions based on peptide-MHC class-II affinities.

Together, this work will generate insights into incompletely understood aspects of CD4+ T cell responses to the live attenuated YFV-17D that will contribute to a better understanding of the mechanisms that influence epitope specificity and immunodominance.

3. Results

3.1. The CD4+ T cell response to YFV structural proteins C, prM/M and E

To define the CD4+ T cell specificities in humans vaccinated with the live attenuated yellow fever vaccine (YFV-17D), we first determined the overall extent of CD4+ T cell responses to the structural proteins C, prM/M and E. PBMC samples from 76 YFV-17D vaccinees were restimulated with pools of overlapping 15-mer peptides which cover the entire sequence of each protein and analysed in interleukin-2 (IL-2) enzyme-linked immunosorbent spot (ELISPOT) assays. The rationale to employ an IL-2 ELISPOT was based on previous findings which indicated that the frequency of IL-2-secreting virus-specific CD4+ T cells correlates with the magnitude of antibody titers (5, 58, 107).

As shown in Fig. 3.1-1 A, the CD4+ T cell response magnitude varied strongly between individuals (e.g. E-specific spots ranging from 7 to 185 per $1x10^6$ CD8-depleted PBMCs) and also between the three structural proteins (Kruskal-Wallis test, P<0,0001 and Dunn´s multiple comparisons test). There was a strong correlation between the magnitudes of C and E protein-specific CD4+ T cell responses although the ratios of E- to C-specific responses showed a considerable individual variation ranging from 0.5 to 15.2 (Fig. 3.1-2).

To test the specificity of the assay, we investigated CD4+ T cell responses of ten YFV-naive individuals. As can be seen in Fig. 3.1-1 A, the YFV-naïve individuals did not mount a specific response to any of the YFV peptide pools. We next analysed the contribution of peptides from the three structural proteins to the total CD4+ T cell response. As shown in Fig. 3.1-1 B, E peptides contributed 60.3% of the overall response whereas prM/M and C peptides contributed 12.4% and 27.3%, respectively. Considering the molecular weight ratio in mature (Fig. 3.1-1 C) or immature (Fig. 3.1-1 D) particles, capsid-specific CD4+ T cell responses are overrepresented approximately two-fold compared to the envelope proteins (ELISPOT: C to prM/M and E = 0.37; molecular weight: C to prM/E = 0.16, C to M/E 0.19).

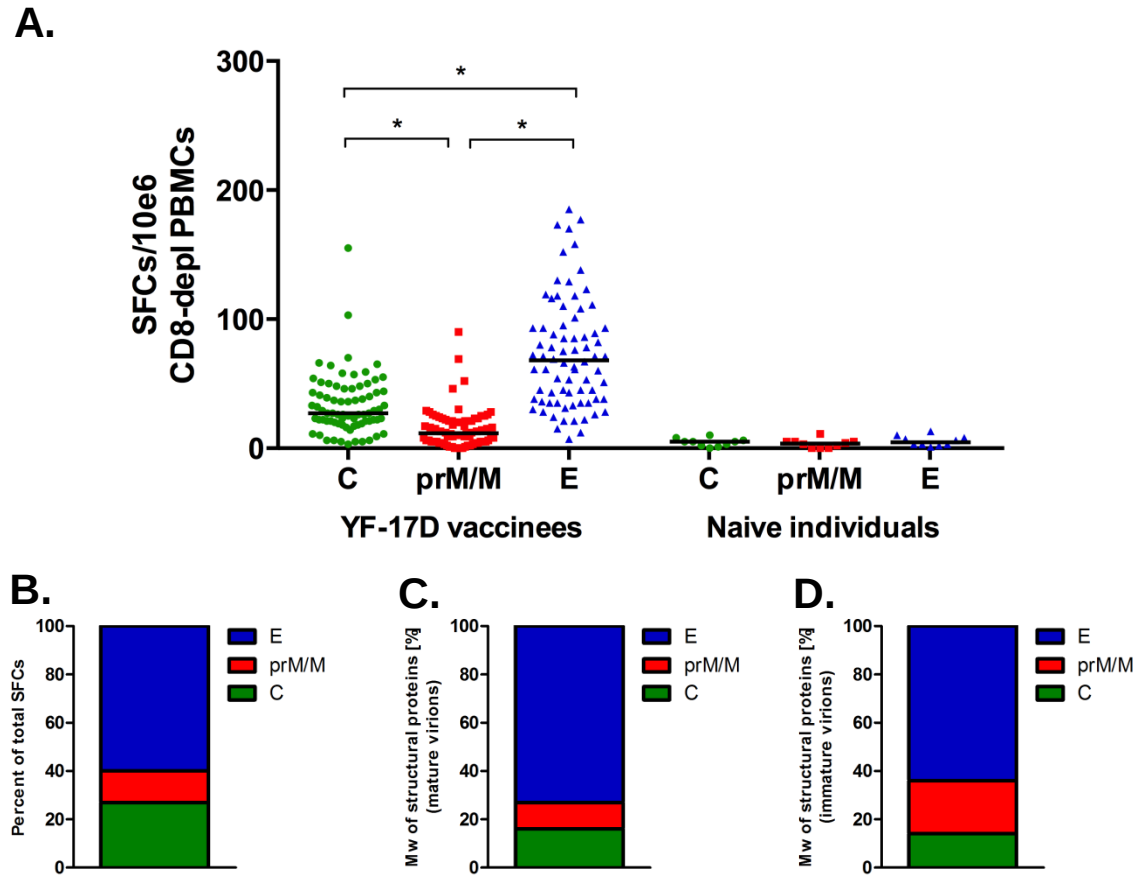

Fig. 3.1-1 Magnitude of CD4+ T cell responses against YFV structural proteins. (A) Individual CD4+ T cell responses to C, prM/M and E were determined in PBMCs from YF-17D vaccinated (n=76) and YFV-naïve humans (n=10). Interleukin-2 (IL-2) ELISPOT results are shown as spot forming cells (SFCs)/1x10^6 CD8-depleted PBMCs. Statistical comparisons were performed using a Kruskal-Wallis test (P<0,0001) and Dunn´s multiple comparisons test. Significant differences are indicated by stars. Medians are indicated by black lines. (B) Percent of total SFCs established by C, prM/M and E-specific CD4+ T cells. (C and D) Molecular weight distribution of YFV structural proteins C, prM/M and E assuming fully mature (C) and immature (D) virus particles.

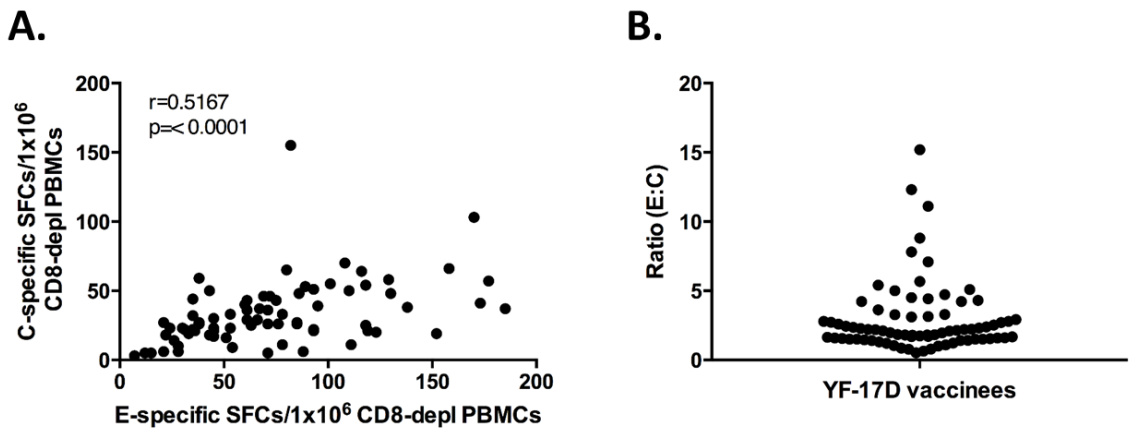

Fig. 3.1-2 Individual magnitude of C and E-specific CD4+ T cell responses. (A) Spearman correlation of individual (n=76) C- and E-specific CD4+ T cell responses from YFV-17D vaccinees. (B) E/C ratios of individual CD4+ T cell responses (n=76; values below the cutoff of 21 SFCs/1x10^6 CD8-depleted PBMCs were set to 10 for this analysis).

3.2. Epitope-specificity of CD4+ T cell responses to C, prM/M and E proteins

To determine the fine-specificity of CD4+ T cell responses in YFV-17D vaccinated individuals, we employed matrix pools and single peptides covering the complete amino acid sequences of C, prM/M and E proteins in IL-2 ELISPOT assays. Figure 3.2-1 illustrates individual CD4+ T cell responses to YFV structural proteins C and E in three representative examples. We found that individual CD4+ T cell responses were restricted to limited sets of peptides and that individual epitope profiles exhibited considerable variation.

To obtain information on immunodominance patterns of the study cohort, we calculated the frequency of obtaining a positive ELISPOT result for each peptide. This frequency is depicted as the percentage of responders out of all individuals recognizing at least one peptide of the corresponding protein. Within the study cohort, we identified three peptides in the C protein and five peptides in the E protein that elicited a CD4+ T cell response significantly more often (chi-square, $p<0.05$) than the average of peptides from the respective protein (indicated by asterisks and bold numbers in Fig. 3.2-2). These eight peptides were therefore defined as immunodominant.

Consistent with the low overall response magnitude to the prM/M peptide pool (Fig. 3.1-1), the corresponding single peptides yielded only a few positive signals, and thus, meaningful statistical analysis of prM/M fine-specificities was not possible.

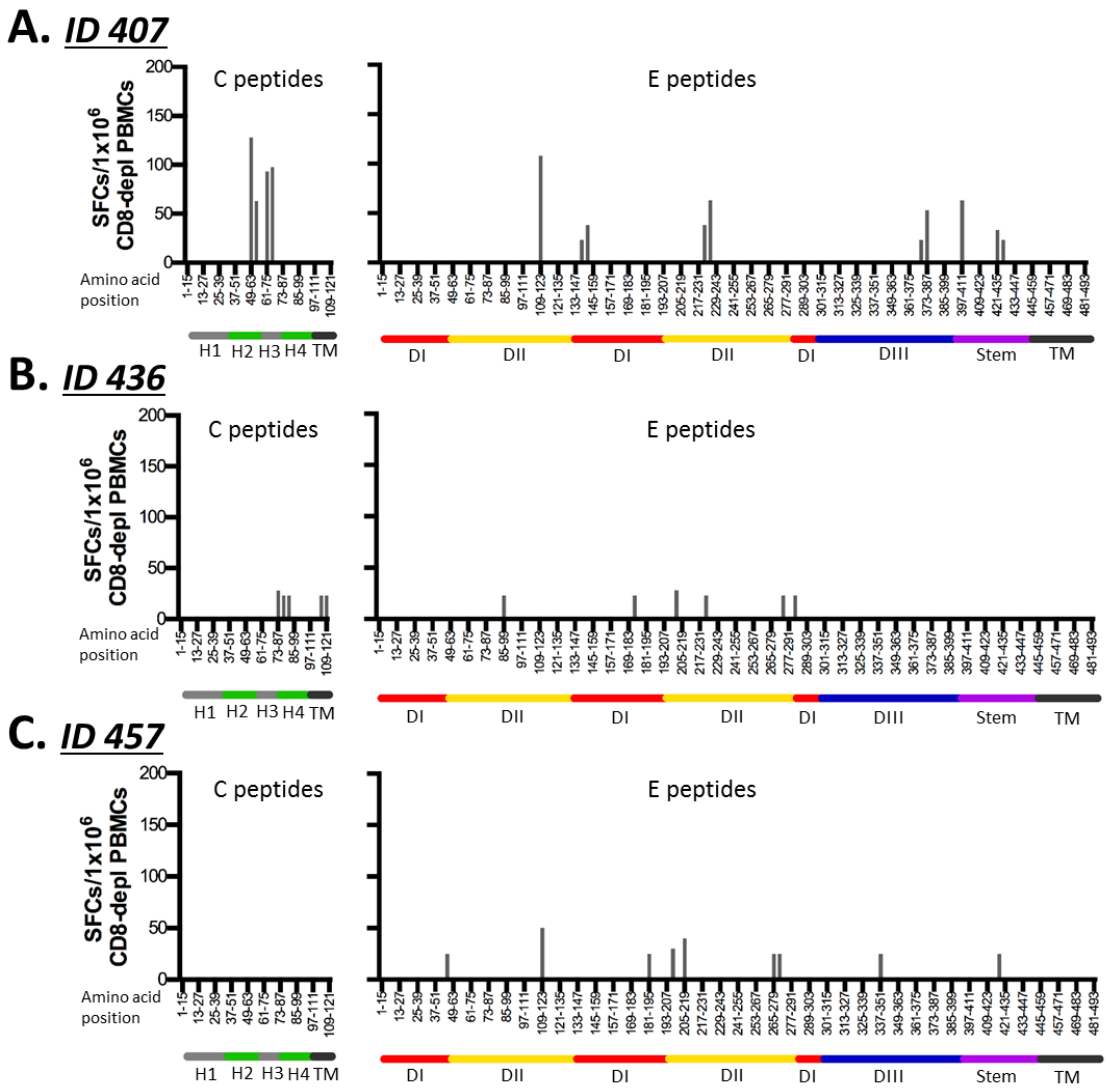

Fig. 3.2-1 Individual variation of CD4+ T cell epitope specificities to YFV C and E proteins. CD4+ T cell responses to C (left panels) and E (right panels) were determined in an IL-2 ELISPOT assay using 15-mer peptides. (A-C) The CD4+ T cell epitope specificities of three YFV-17D vaccinated individuals are shown as spot forming cells (SFCs)/1x10^6 CD8-depleted PBMCs. No positive responses to prM/M peptides were observed in the individuals shown. Amino acid positions of peptides refer to their appearance in the sequence of C and E, respectively. Colored bars below C protein x-axes show positions of alpha helices 1 to 4 (grey and green) and the transmembrane (TM; black) ER anchor. Envelope protein domains are colored in red (DI), yellow (DII), blue (DIII), purple (stem) and black (transmembrane domain, TM).

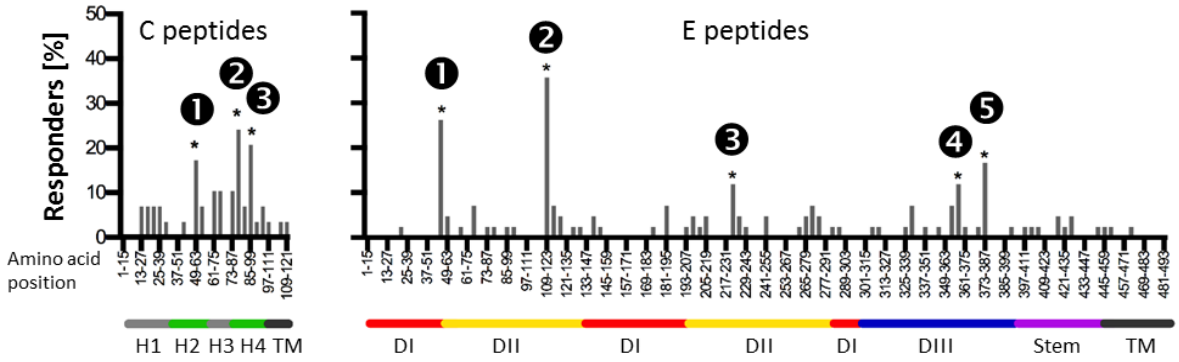

Fig. 3.2-2 Cumulative epitope specificities of YF-17D vaccinees with at least one peptide response. Percentage of YFV-17D vaccinees recognizing a specific peptide within C (n=29) and E (n=42) proteins. Peptides recognized significantly more often than the average (Fisher´s exact or chi-square test; significance level of $P<0.05$; separately for each protein) are indicated by asterisks and numbers. Amino acid position of employed peptides within the protein sequence are indicated below the x-axis. Colored bars represent corresponding protein domains as in Fig. 3.2-1.

3.3. Analysis of dominant epitopes in the context of three-dimensional C and E protein structures

Structural features of complex protein antigens can influence the specificity of CD4+ T cell responses (19, 49, 53, 68, 107, 122). Thus, experimentally identified immunodominant epitopes were analyzed in the context of the three-dimensional (3D) structures of C and E proteins. Since these flavivirus proteins are structurally conserved (26, 59, 61, 72, 86, 94) and structural data does not exist for YFV proteins, epitopes were assigned to the available homologous crystallographic structures of Kunjin virus (KUNV) C protein (26) and tick-borne encephalitis virus (TBEV) E protein (94).

The CD4+ T cell response to the C protein was strongly focused to helices two and four whereas helices one and three as well as the N-terminal region had much lower representation or did not elicit any response (Fig. 3.3-1).

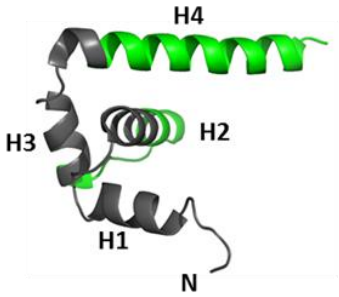

Fig. 3.3-1 Mapping of dominant CD4+ T cell responses to the C protein. Crystallographic structure of flavivirus Kunjin C protein comprising four alpha helices (H1 to H4) (26). For the N-terminal region (gray line), no crystallographic data exists. Dominant CD4+ T cell epitopes are highlighted in green.

In the E protein, the five immunodominant peptides are located in domain I, II and III and span different secondary structures such as beta sheets and loops (Fig. 3.3-2). Dominant epitopes were neither found at the very C-terminus nor the C-terminal stem and transmembrane (TM) helices of the E protein.

Interestingly, all five dominant peptides were located on the exposed surface of E protein dimers (Fig. 3.3-2). Structural rearrangements of the E protein dimer which mediate fusion can occur at the pH of early endosomes. Thus, also trimeric post-fusion E proteins may be relevant substrates for antigen processing and presentation. The allocation of immunodominant epitopes revealed that all immunodominant epitopes were also accessible on the surface of E protein trimers (Fig. 3.3-3). Therefore, accessibility of these protein regions to proteolytic processing and/or MHC-II binding may have facilitated the selection of these epitopes.

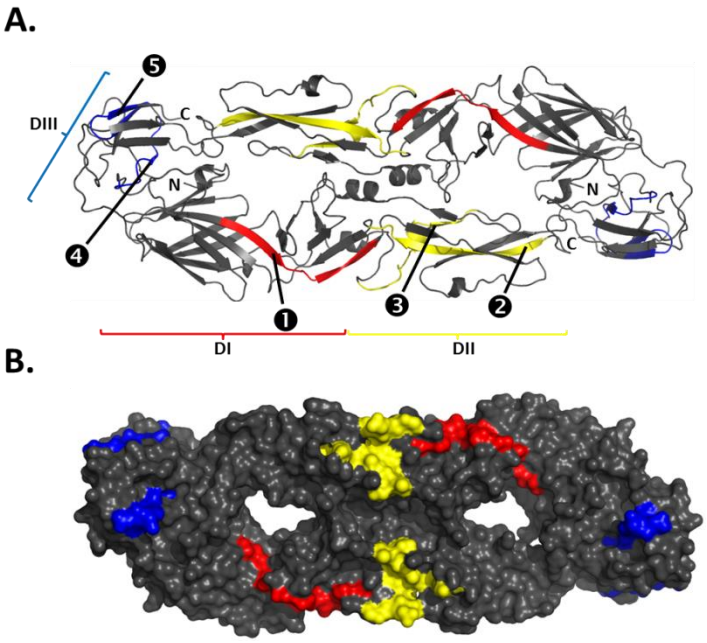

Fig. 3.3-2 Mapping of dominant CD4+ T cell responses to the E protein dimer. (A and B) Crystallographic structure of the TBEV soluble envelope (sE) protein consisting of three domains (DI-III) (94). Immunodominant peptides are colored in both monomers according to corresponding domains: DI (red), DII (yellow) and DIII (blue). (A) Ribbon representation of sE. (B) Surface view of sE.

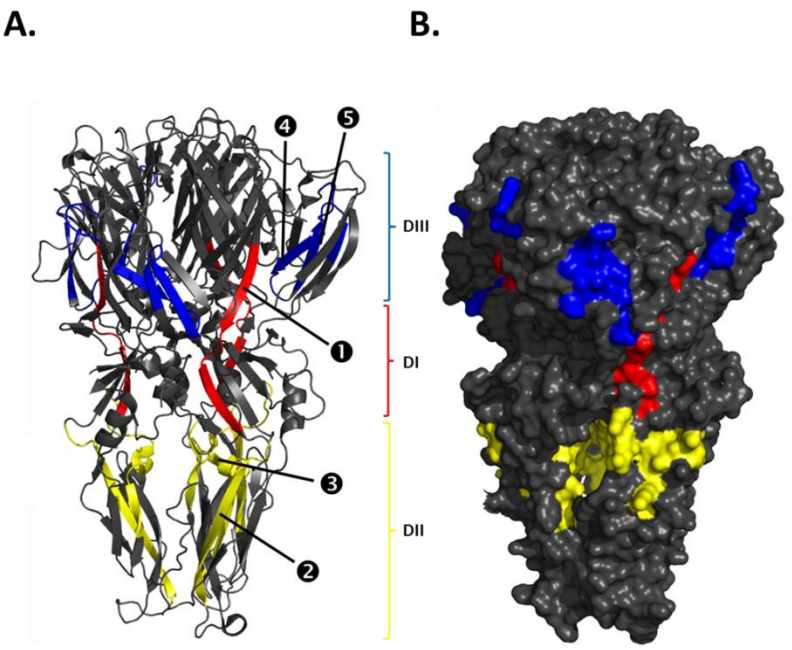

Fig. 3.3-3 Mapping of dominant CD4+ T cell responses to the E protein trimer. (A and B) Crystallographic structure of TBEV sE protein trimer (17). Dominant CD4+ T cell epitopes are colored in red (DI), yellow (DII) and blue (DIII). (A) Ribbon diagram of TBEV sE trimer. (B) Surface representation of TBEV sE trimer.

3.4. *In silico* epitope prediction for YFV structural proteins C and E

Presentation of peptides via MHC-II molecules is a pre-requisite for the activation of CD4+ T cells and peptide-MHC-II binding affinity is an important factor for the selection of immunodominant epitopes (51, 129). We investigated the relationship between the experimentally determined CD4+ T cell epitopes and the *in silico* predicted peptide-MHC-II binding affinity. For this purpose, we performed genotyping of HLA alleles from all individuals. The results are shown in Table 3.4.

This analysis is still in progress and therefore, a reference set of 27 HLA class-II alleles which covers 99% of specificities present within the human population (33, 39) was used to predict the top ten percent binding peptides in the C and E proteins of YFV. The Immune Epitope Database (IEDB) calculates a percentile rank for 15-mer peptides to predict the binding affinity to HLA-II (39).

Results shown in Fig. 3.4 reveal that all immunodominant CD4+ T cell epitopes were also indicated in the MHC-II binding prediction. Each dominant peptide of C and E proteins was predicted for at least 2 alleles. Especially in the C protein, we found good congruence between predicted and experimentally identified epitopes. The experimentally identified epitopes were predicted for a high number of HLA alleles

(up to 18/27). In the E protein, experimentally identified epitopes were less frequently predicted as top binder for many HLA alleles (up to 6/27). On the other hand, many frequently predicted peptides (e.g. in transmembrane domains, TM) were not confirmed experimentally (Fig. 3.4).

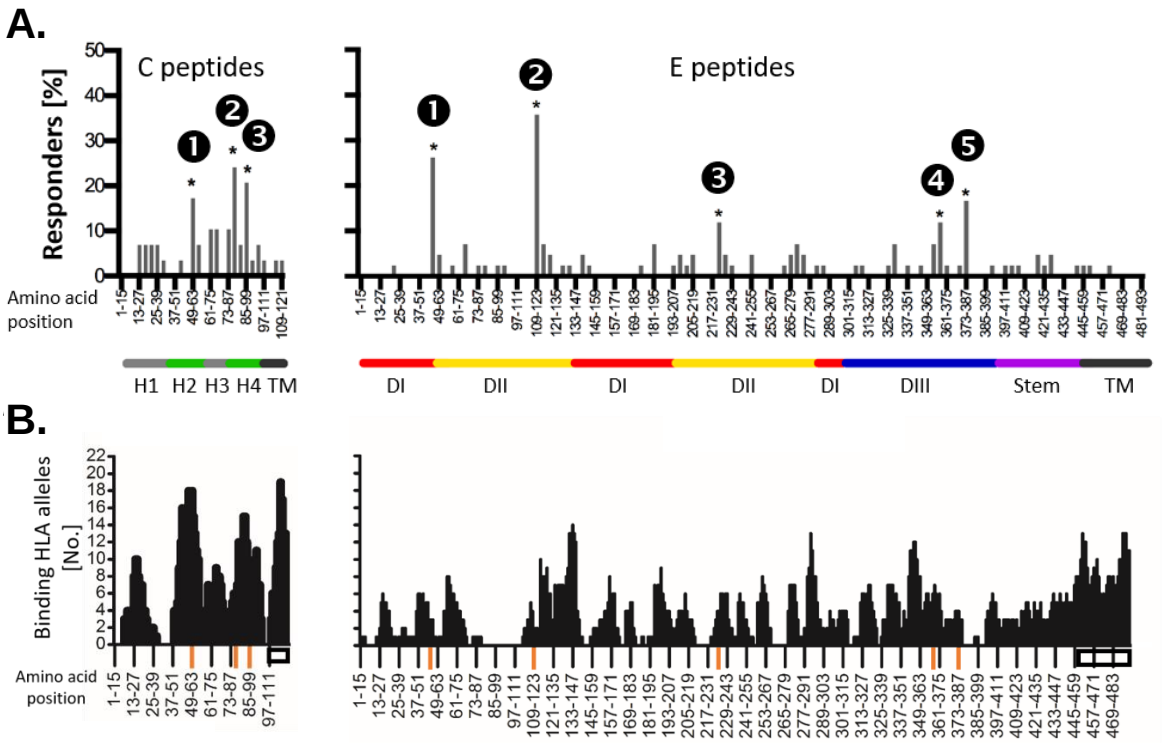

Fig. 3.4 Experimentally identified YFV epitopes and *in silico* peptide-MHC-II binding predictions for C and E proteins. (A) Experimentally determined CD4+ T cell epitopes. Bold numbers are dominant CD4+ T cell epitopes. (B) *In silico* prediction of epitopes for a reference set of 27 HLA alleles (33, 39). Orange bars indicate positions of dominant YFV epitopes as determined in IL-2 ELISPOT assays. Black rectangles indicate transmembrane domains (TM).

Table 3.4 Individual HLA class-II alleles.

ID	DRB1		DQB		DPB	
403	11:04:01	13:01:01	06:03:01		02:01:02	04:01:01
405	03:01:01:01	11:04:01	02:01:01	03:01:01:03	04:02:01	14:01:01
407	01:01:01	08:01	04:02:01	05:01:01:03	04:01:01	
410	01:01:01	15:01:01:03	05:01:01:03	06:02:01		
412	03:01:01:01	13:01:01	06:03:01		03:01:01	19:01
413	04:02:01	11:04:01			04:01:01	
415	13:01:01		06:03:01		10:01	
416	07:01:01	15:01:01	03:03:02:01	06:03:01	02:01:02	10:01
417	01:01:01	07:01:01:01	05:01:01:03			
418	04:04:01	15:01:01	03:02:01	06:02:01	04:01:01:01	23:01:01
420	11:01:02	13:01:01	05:02:01	06:03:01	01:01:01	04:01:01
421	15:01:01:01	16:02:01	05:02:01	06:02:01		
422	13:02:01	15:01:01:01				
424	11:01:01		03:01:01:03		04:01:01	20:01:01
425	01:01:01	11:04:01	05:01:01:03		02:01:02	04:01:01:01
426	13:02:01	15:01:01			04:01:01	06:01
427	04:01:01	13:01:01	03:02:01	06:03:01	04:01:01:01	
428	01:01:01	13:01:01	05:01:01:03	06:03:01	02:01:02	04:01:01
429	08:03:02	15:01:01:01	06:01:01	06:02:01	02:01:02	05:01:01
430	03:01:01:01	08:04:01	02:01:01	03:19	01:01:02	85:01
432	04:01:01	15:01:01:01	03:02:01	06:02:01		
434	01:01:01	15:01:01:03	05:04	06:02:01	04:01:01:01	05:01:01
436	01:01:01	15:02:01	05:01:01	06:01:01		
437	07:01:01	11:01:01	02:02:01	03:01:01	01:01:01	04:01:01
438	15:01:01:01	16:01	05:02:01	06:02:01	04:01:01	
440	01:01:01	07:01:01	05:01:01:03			
441	04:01:01	15:01:01	03:02:01	06:02:01	04:01:01:01	
444	11:01:01	15:01:01	06:02:01		04:01:01	
445	03:01:01	11:04:01	02:01:01	03:01:01		
447	03:01:01	07:01:01	02:01:01	02:02:01	01:01:01	14:01:01
449	03:01:01	04:04:01	02:01:01	03:02:01	04:01:01	
451	04:01:01	15:01:01	06:02:01		04:01:01	
452	03:01:01	04:01:01	02:01:01	03:01:01	01:01:01	04:01:01
454	13:01:01	15:01:01	06:02:01	06:03:01	04:01:01	
455	04:01:01	08:01	03:01:01:01	04:02:01		
457	03:01:01:02	07:01:01:01	02:01:01	02:02:01	02:01:02	
460	04:08:01	11:01:01	03:01:01:01	03:01:01:03	03:01:01	
461	03:01:01:01	04:01:01	03:02:01			
462	03:01:01:02	13:01:01	06:03:01		01:01:01	04:01:01
463	11:01:01	13:01:01	06:03:01		03:01:01	04:02:01
464	04:01:01		03:02:01		04:01:01	
466	03:01:01:01	13:01:01	06:03:01		01:01:01	02:01:02
467	04:01:01		06:04:01			
468	07:01:01	11:01:01	03:01:01	03:03:01	02:01:02	04:01:01
469	15:01:01	13:01:01	06:02:01	06:03:01		
470	01:02:01	04:04:01	03:02:01	05:01:01:01	03:01:01	104:01
471	15:01:01:01	16:01:01	05:02:01	06:02:01		
473	01:01:01	03:01:01	05:01:01:03		04:02:01	15:01:01
475	11:04:01		03:01:01:03		04:01:01	
476	03:01:01:01	04:01:01	03:02:01			
477	03:01:01:01	04:01:01	03:02:01			
478	11:01:01	15:01:01:02	06:02:01		04:01:01	
479	11:01:01		03:01:01		02:01:02	04:01:01:01
479			03:01:01:03		02:01:02	04:01:01:01
481	01:01:01	04:01:01	03:02:01	05:01:01	02:01:02	04:01:01
482	11:01:01	13:01:01	06:03:01			
483	01:01:01	07:01:01:02	03:03:02:01	05:01:01:03	04:01:01:01	23:01:01
486	04:01:01		03:02:01	06:03:01		
487	04:01:01	07:01:01			04:01:01	16:01:01
488			02:01:01	03:01:01		
489	11:01:01	15:01:01	03:01:01:03	06:02:01	04:01:01:01	
490	04:01:01	16:01:01	03:02:01	05:02:01	04:02:01	
491	01:01:01	11:01:01	05:01:01:03	03:01:1:03	01:01:01	04:01:01
495	07:01:01	11:01:01	02:02:01	03:01:01	02:01:02	04:01:01
496	03:01:01	16:01:01	02:01:01	05:02:01	01:01:01	04:01:01
498	11:03		03:01:01:03		03:01:01	04:02:01:02

3.5. Comparative analysis of CD4+ T cell epitopes identified in the three-dimensional structures of flavivirus C and E proteins

To identify general features of structure-related epitope patterns in flaviviruses, the dominant epitope regions identified in YFV C and E proteins were compared to those previously identified within TBEV (107).

Inspection of the data shown in Fig. 3.5 A revealed that in the C protein dominant peptides identified in YFV and TBEV were located at almost identical positions in the presumptive helices two and four. Also in the E protein, immunodominant YFV peptides in domain I (1), domain II (3) and domain III (4) were congruent with dominant TBEV epitopes (Fig. 3.5 B). Immunodominant YFV epitope number 5 (domain III) resides adjacent to a dominant TBEV epitope. One dominant YFV peptide (2) was not identified in the TBEV E protein.

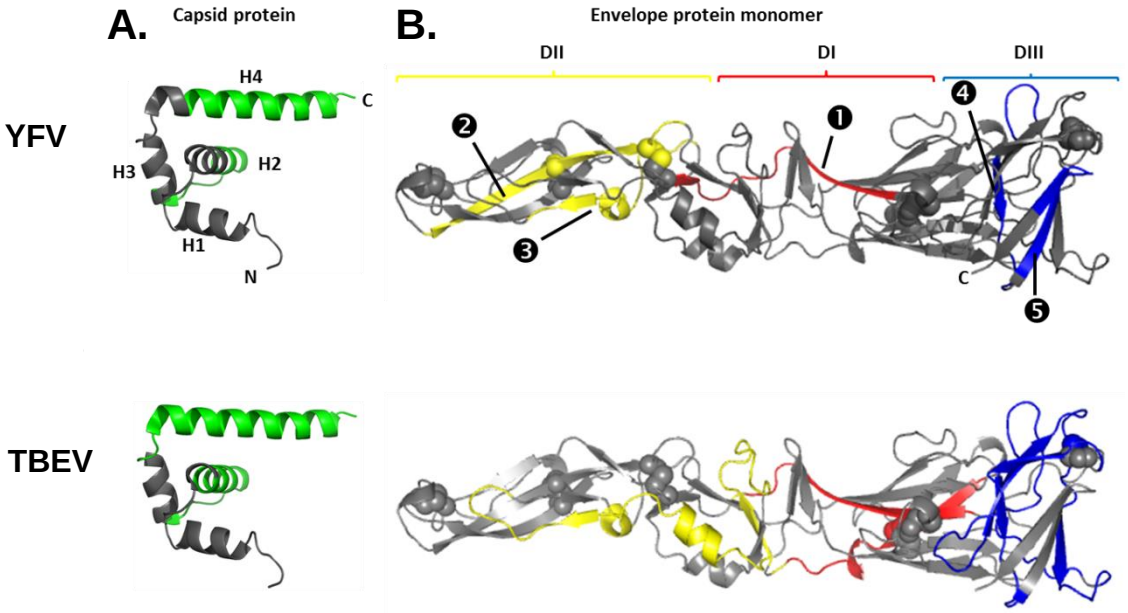

Fig. 3.5 Location of dominant CD4+ T cell epitopes identified after YFV and TBEV vaccination. (A) Crystallographic structure of KUNV C protein (26). (B) Crystallographic structure of TBEV sE protein (94). Dominant peptides are colored as follows: C protein (green); E protein DI (red), DII (yellow) and DIII (blue), spheres represent disulfide bridges.

3.6. Analysis of neutralizing antibody responses to YFV

To investigate whether CD4+ T cell responses to YFV structural proteins correlate with antibody responses, we determined YFV-specific neutralizing antibody titers in sera from all study participants. We found a positive correlation for individual YFV-specific neutralizing antibody titers and the magnitude of CD4+ T cell responses against capsid (C) and envelope (E) proteins as determined by IL-2 ELISPOTs (Fig. 3.6).

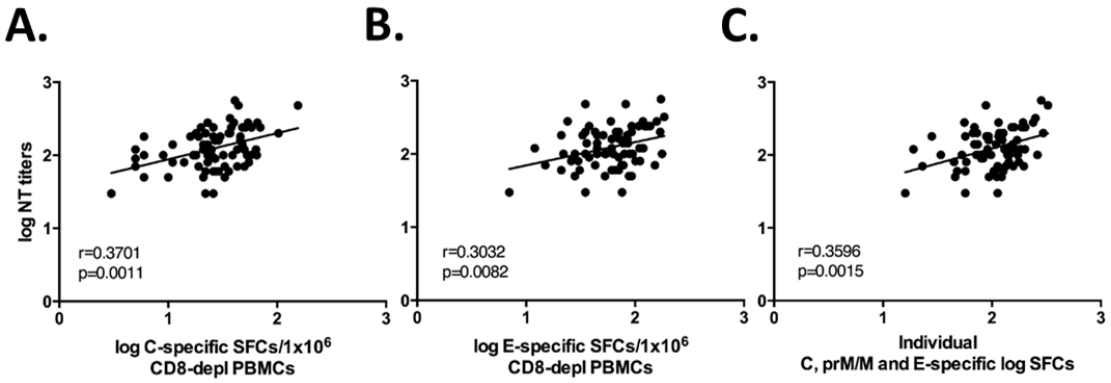

Fig. 3.6 Correlation of individual neutralizing antibody and CD4+ T cell responses to YFV. The magnitude of CD4+ T cell responses to YFV C protein (A), E protein (B) as well as C, prM/M and E proteins together (C) was plotted against the corresponding YFV neutralizing antibody titers (n=76). Statistical analysis was done using Spearman correlation. Linear regressions are indicated by a black line.

3.7. Other factors that could influence CD4+ T cell responses

We also analysed other factors such as age, sex and the time interval between vaccination and sample collection that could potentially influence the CD4+ T cell response. Age is associated with alterations in hematopoietic stem cells which results in decline of immune responsiveness which may also impair immunity after infection or vaccination (9, 57). Accordingly, we tested whether CD4+ T cell responses following live attenuated YFV-17D vaccination decline with age. However, no significant correlation was observed in our study cohort (Fig. 3.7). Moreover, we found similar CD4+ T cell response magnitudes between female and male participants (Fig. 3.7). To investigate whether the frequency of YFV-specific IL-2 producing CD4+ T cells is influenced by the time interval between vaccination and sample collection, we correlated the days between vaccination and blood collection with the magnitude of responses. However, there was no correlation between these parameters (Fig. 3.7).

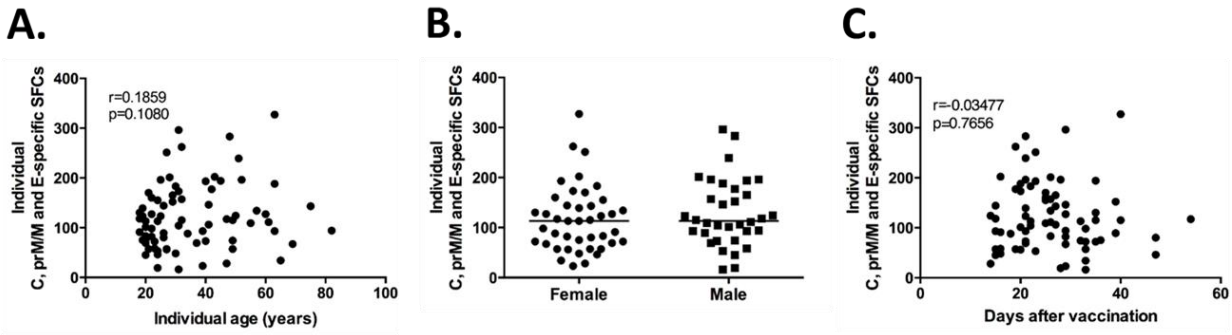

Fig. 3.7 Relation of age, sex and time point of blood collection after YFV-17D vaccination and the magnitude of CD4+ T cell responses. (A) Correlation of age at the time point of sample collection and the magnitude of CD4+ T cell responses. (B) Comparison of CD4+ T cell responses between female and male vaccinees. (C) Correlation of CD4+ T cell responses and days between vaccination and sample collection. The statistical analysis is shown on the top left corner (Spearman correlation).

4. Discussion

In this study, we determined the overall extent and fine-specificities of CD4+ T cell responses to YFV structural proteins C, prM/M and E in PBMCs from 76 YFV-17D vaccinees. The experimentally identified epitopes were analyzed in relation to the three-dimensional structures of C and E proteins, and to *in silico* epitope predictions based on peptide-MHC-II affinities.

Overall, the CD4+ T cell responses were chiefly directed against the E protein followed by C- and prM/M proteins (Fig. 3.1-1 A and B). Considering the molecular weight distribution of YFV structural proteins, capsid-specific responses were approximately two times overrepresented (Fig. 3.1-1 B, C and D). Theoretically, intrinsic properties of the C protein could generate a propensity to favor MHC-II-restricted presentation of C peptides and T cell activation. However, a previous study with TBEV revealed a three-fold molar excess of C over prM/M and E in virus particles (107). The experimentally determined responses were therefore concordant with the amount of these proteins in the virion. This suggests that peptides of the three structural YFV proteins contribute equally to the CD4+ T cell responses relative to the protein amounts in the virion.

Neutralizing antibody responses directed against the major envelope protein E are an accepted correlate of protection against flaviviruses (91). As reported for HBV and influenza virus, envelope-specific B cells can internalize virus particles and subsequently present peptides of envelope and internal proteins in complex with MHC class-II molecules (65, 105, 106). For flavivirus neutralizing antibody responses, such CD4+ helper T cell epitopes can be derived not only from envelope (E) proteins but also from the other two structural proteins C and prM/M (62, 97, 107) which may be co-internalized as part of the virus particle by E-specific B cells. Accordingly, CD4+ T cell responses directed against all three structural proteins can provide help to E-specific B cells producing neutralizing antibodies. Consistent with these considerations, we observed a significant correlation between the titers of YFV-neutralizing antibodies and the extent of CD4+ T cell responses directed against YFV envelope and capsid proteins in YFV-17D vaccinated individuals (Fig. 3.6).

The analysis of the complete repertoire of CD4+ T cell epitope specificities in response to C, prM/M and E showed that in each of these proteins only a few peptides were selected as CD4+ T cell epitopes. These epitopes varied considerably between individual YFV-17D vaccinees. The response to membrane (prM/M)

peptides was very low and therefore a meaningful interpretation of immunodominant epitopes in prM/M was not possible. Weak CD4+ T cell responses to prM/M have been also reported for dengue virus and TBEV (97, 107). For E and C proteins, certain epitope regions were recognized significantly more often and were therefore defined as immunodominant.

When we analyzed the experimentally identified epitopes with respect to their location in the protein structures using the homologous crystallographic structures of C and E, we found that in the C protein, CD4+ T cell responses were focused to helices two and four whereas helices one and three and the conformationally unstable N-terminal region did not elicit frequent CD4+ T cell responses (Fig. 3.3-1). A comparison between the crystallographic structure of KUN C protein and the NMR structure of DENV2 C protein revealed a similar orientation of helices 2, 3 and 4 to each other whereas orientation of helix 1 to helix 2 was different (26). Thus, conformational stability of the C protein likely influenced the specificity of CD4+ T cell responses as it has been shown for influenza virus hemagglutinin (49).

In the envelope protein, epitopes were identified in all three domains (Fig. 3.3-2). Interestingly, all dominant epitopes of the E protein were located at the exposed protein surface of the E protein. This finding is in agreement with previous studies in HIV and influenza virus that identified epitope clusters at exposed protein surfaces or at flanks of protease-sensitive loops (19, 49, 81), suggesting that accessibility of protein regions to endosomal cleavage and/or MHC-II binding may facilitate the selection of CD4+ T cell epitopes.

After receptor-mediated endocytosis of flavivirus particles, E proteins undergo substantial acidic pH-induced rearrangements that enable the fusion with endosomal membranes (17, 115). Since the conversion of E protein dimers into post-fusion trimers can occur at the acidic pH of early endosomes, these conformational changes may alter the availability of epitopes to proteolytic processing and/or MHC-II binding. An analysis of the immunodominant epitopes in the context of the E protein trimer revealed that all immunodominant epitopes were also accessible on the surface of E protein trimers (Fig. 3.3-3). Taken together, the analysis of experimentally identified epitopes in the tertiary protein structures of flaviviruses suggest that the selection of dominant epitopes is influenced by features of the three-dimensional antigen structure.

To obtain further insights into possible structural factors that influence the specificities of CD4+ T cell responses to flaviviruses, we compared the dominant epitope sites identified in YFV C and E proteins with those previously determined for the related TBEV (107). This comparison showed that all (3/3) of the C epitopes and 60% (3/5) of E epitopes identified in YFV overlap with those identified in TBEV (Fig. 3.5). Given that flavivirus proteins have a conserved structure but share only 40% identical amino acids, our results suggest a structural influence on endosomal epitope selection and immunodominance of CD4+ T cell responses.

An additional CD4+ T cell epitope was identified in the YFV E protein that is located in sequence elements forming a β-sheet at the tip of domain II (amino acid position 109-123) that is stabilized in the tertiary E protein structure by two disulfide bridges. It has been shown that such stable epitopes require gamma-interferon-inducible lysosomal thiol reductase (GILT) activity in order to become available for antigen presentation (53, 67, 81). This epitope was immunodominant only in YF vaccinees but not in TBEV infected or vaccinated individuals. *In silico* predictions of MHC-II binding affinities revealed that this epitope was rarely predicted for YFV as well as for TBEV amino acid sequences. This indicates that the difference in the dominance of this epitope was not due to a difference in peptide-MHC-II affinity between YFV and TBEV.

Peptide-MHC-II affinity-based *in silico* epitope predictions are often used for the pre-selection of CD4+ T cell epitope candidates prior to experimental determination (21, 127, 130). Several studies indicate that high peptide-MHC-II affinity is an important determinant of epitope presentation and also of subsequent CD4+ T cell epitope specificities (51, 103, 129). Epitope prediction in YFV C, prM/M and E proteins revealed many potential epitopes. However, the extent to which predicted epitopes matched the experimental data varied strongly between proteins and specific structures within these proteins (Fig. 3.4). We observed a good match in the C protein (i.e. immunodominant epitopes were predicted to bind more than 50% of analyzed HLA alleles with high affinity). In contrast, dominant epitopes from the E protein were predicted as high affinity MHC-II binders only for ~20% of HLA alleles. On the other hand, none of the most frequently predicted epitopes in E (i.e. predicted in >50% of alleles) were identified experimentally. For instance, high affinity peptides were frequently predicted in transmembrane domains but corresponding CD4+ T cell specificities were not dominant in ELISPOT assays. Since flavivirus transmembrane

sequences can principally elicit CD4+ T cell responses (38), structural impairment of antigen processing and presentation by shielding within lipid membranes appears possible. In fact, current in silico class-II epitope prediction programs do not consider proteolytic processing or TCR recognition but peptide-MHC class-II affinity only (20). These findings are in agreement with previous studies with HIV and EBV which demonstrated that epitope dominance does not correlate with high MHC II affinity (14, 123). Thus, such epitope predictions can miss important epitopes which are not selected predominately on the basis of peptide-MHC-II affinity.

In summary, the work of this thesis provides new insights into the CD4+ T cell specificities and immunodominance patterns induced by the live attenuated YFV vaccine. Moreover, our data suggest that antigen structure is an important determinant that influences the selection of dominant epitopes in addition to peptide-MHC-II affinity. In order to delineate improved models for the prediction of dominant class-II epitopes, future studies should generate additional direct mechanistic insights to pin down the contribution of three-dimensional protein structures to the specificity of CD4+ T cell responses.

5. Materials and Methods

5.1. Donors

5.1.1. YFV-17D vaccinees

The study cohort (table 5.1.1) comprised 76 humans (42 females and 34 males; age range 18-82 years, median age 31 years) who had been vaccinated with the live attenuated yellow fever virus strain 17D-204 (STAMARIL®; Sanofi Pasteur). Previous infection and/or vaccination with TBEV was excluded using TBEV-specific neutralization assays. None of the individuals had a health condition such as acute infection or immunotherapy which could have distorted T cell responses. Peripheral blood samples were obtained 14-54 days (median 25 days) after vaccination. Yellow fever vaccination as well as blood collections were performed at the Eppendorf Klinik, Hamburg. Whole blood was collected in sodium citrated tubes to avoid coagulation. The study was approved by the ethical committee of the medical association Hamburg (approval number PV4513). Written informed consent was obtained from all study participants.

Table 5.1.1 Demographic characteristics of YF-17D vaccinees (n=76).

Sample ID	Age [years]	Days between vaccination and blood sampling	Sex [male/female]
403	34	18	f
405	52	28	m
407	31	29	m
409	69	29	f
410	27	23	f
412	45	35	m
413	19	21	m
415	30	22	f
416	49	19	f
417	26	39	m
418	31	22	m
420	40	21	m
421	61	26	m
422	57	26	f
424	41	27	m
425	27	33	f
426	31	33	m
427	75	27	f
428	18	35	f
429	32	35	f
430	41	29	m
431	82	29	m
432	60	29	f
434	30	16	f
436	32	26	m
437	40	23	f
438	29	39	m
440	63	40	f
441	49	40	m
444	22	25	f
445	47	54	f
447	23	33	f
449	65	33	f
450	22	33	f
451	24	47	f
452	26	47	f
453	24	28	m
454	24	25	f
455	51	21	m
457	25	21	m
458	48	21	m
460	22	29	f
461	20	26	f
462	32	19	f
463	42	19	m
464	22	29	f
465	39	29	f
466	63	21	m
467	55	25	m
468	20	15	m
469	20	20	m
470	18	16	f
471	27	20	f
473	23	16	m
475	24	22	f
476	19	36	f
477	29	27	m
478	28	26	m
479	37	21	f
480	47	14	f
481	50	14	m
482	20	35	f
483	21	25	f
484	25	21	f
486	20	21	m
487	18	15	m
488	19	21	f
489	63	20	m
490	20	32	f
491	49	32	m
493	39	15	m
494	31	20	f
495	24	23	m
496	43	16	f
498	21	15	f
500	26	15	f
Range	18-82	14-54	42f/34m
Median	31	25	

5.1.2. YFV-naïve individuals

For assay validation, YFV-specific T cell responses were assessed in human peripheral blood samples from a group of ten YF-naive individuals (6 females and 4 males; age range 22-47 years, median age 23 years). At the day of sample collection, none of the participants had exhibited a health condition such as acute infection, which could have influenced CD4+ T cell responses. Previous infection and/or vaccination with YFV and TBEV was excluded in all 10 subjects using neutralization assays. Blood collections were performed at the Department of Virology of the Medical University of Vienna, Vienna.

5.1.3. Assay control

As an assay control, samples from a healthy anonymous TBEV vaccinated donor was obtained from the “Blutspendezentrale für Wien, NÖ und Burgenland”. The blood bag contained citrate buffer as anticoagulant.

5.2. Preparation of PBMCs for T cell assays

Peripheral blood mononuclear cells (PBMCs) were isolated from whole blood samples by density gradient centrifugation using Ficoll-Paque Plus™ (GE Healthcare) and cryopreserved in liquid nitrogen for future use. Corresponding plasma samples were stored at -20°C.

5.3. Depletion of CD8-positive cells

PBMCs were thawed and diluted 1:10 in RPMI 1640 medium (Sigma) containing CTL Wash Supplement (Cellular Technology Limited), 1% glutamine (Sigma), and 50 units/ml Benzonase (Novagen), according to the instructions of Cellular Technology Limited.

PBMCs were depleted of CD8+ cells using anti-CD8 antibody-coupled magnetic beads and LD columns (Miltenyi Biotec) according to company instructions. The CD8-depleted PBMCs were resuspended in serum-free medium (AIM V; Gibco) and incubated overnight at 37°C in 5% CO_2. Subsequently, cells were counted, centrifuged at 300 x g for 10 minutes and resuspended at a final concentration of 2 x 10^6 cells/ml in AIM V medium. The cell suspension was immediately used in interleukin-2 (IL-2) enzyme-linked immunosorbent spot (ELISPOT) assays.

5.4. Flavivirus peptides

5.4.1. Yellow fever virus peptides

For T cell assays, we purchased 28, 39 and 121 15-mer peptides from JPT (Berlin, Germany) which overlap by 11 amino acids and cover the entire sequences of C, prM/M and E structural proteins from YFV-17D (P03314; table 5.4.1). The purity of all peptides was >70% as determined by high performance liquid chromatography (HPLC). Lyophilized peptides were dissolved in dimethyl sulfoxide (DMSO) at a concentration of 1,25 mg of each peptide per ml and then diluted in AIM-V medium at a concentration of 8µg of each peptide per ml. This Stock solution was kept at -20°C until use.

Peptides were arranged into three Maxi Pools, each covering the entire sequence of C, prM/M and E proteins. Additionally, up to 11 peptides were arranged into Matrix Pools using a two-dimensional matrix approach as described previously (7, 107) and shown in Fig. 5.4.1. To verify positive Matrix Pool results, corresponding samples were tested in independent experiments using single peptides.

Table 5.4.1-1 Peptides of YFV C protein.

aa position	Peptide No.	Sequence
1-15	1	MSGRKAQGKTLGVNM
5-19	2	KAQGKTLGVNMVRRG
9-23	3	KTLGVNMVRRGVRSL
13-27	4	VNMVRRGVRSLSNKI
17-31	5	RRGVRSLSNKIKQKT
21-35	6	RSLSNKIKQKTKQIG
25-39	7	NKIKQKTKQIGNRPG
29-43	8	QKTKQIGNRPGPSRG
33-47	9	QIGNRPGPSRGVQGF
37-51	10	RPGPSRGVQGFIFFF
41-55	11	SRGVQGFIFFFLFNI
45-59	12	QGFIFFFLFNILTGK
49-63	13	FFFLFNILTGKKITA
53-67	14	FNILTGKKITAHLKR
57-71	15	TGKKITAHLKRLWKM
61-75	16	ITAHLKRLWKMLDPR
65-79	17	LKRLWKMLDPRQGLA
69-83	18	WKMLDPRQGLAVLRK
73-87	19	DPRQGLAVLRKVKRV
77-91	20	GLAVLRKVKRVVASL
81-95	21	LRKVKRVVASLMRGL
85-99	22	KRVVASLMRGLSSRK
89-103	23	ASLMRGLSSRKRRSH
93-107	24	RGLSSRKRRSHDVLT
97-111	25	SRKRRSHDVLTVQFL
101-115	26	RSHDVLTVQFLILGM
105-119	27	VLTVQFLILGMLLMT
109-121	28	QFLILGMLLMTGG

Table 5.4.1-2 Peptides of YFV prM/M protein.

aa position	Peptide No.	Sequence
1-15	1	VTLVRKNRWLLLNVT
5-19	2	RKNRWLLLNVTSEDL
9-23	3	WLLLNVTSEDLGKTF
13-27	4	NVTSEDLGKTFSVGT
17-31	5	EDLGKTFSVGTGNCT
21-35	6	KTFSVGTGNCTTNIL
25-39	7	VGTGNCTTNILEAKY
29-43	8	NCTTNILEAKYWCPD
33-47	9	NILEAKYWCPDSMEY
37-51	10	AKYWCPDSMEYNCPN
41-55	11	CPDSMEYNCPNLSPR
45-59	12	MEYNCPNLSPREEPD
49-63	13	CPNLSPREEPDDIDC
53-67	14	SPREEPDDIDCWCYG
57-71	15	EPDDIDCWCYGVENV
61-75	16	IDCWCYGVENVRVAY
65-79	17	CYGVENVRVAYGKCD
69-83	18	ENVRVAYGKCDSAGR
73-87	19	VAYGKCDSAGRSRRS
77-91	20	KCDSAGRSRRSRRAI
81-95	21	AGRSRRSRRAIDLPT
85-99	22	RRSRRAIDLPTHENH
89-103	23	RAIDLPTHENHGLKT
93-107	24	LPTHENHGLKTRQEK
97-111	25	ENHGLKTRQEKWMTG
101-115	26	LKTRQEKWMTGRMGE
105-119	27	QEKWMTGRMGERQLQ
109-123	28	MTGRMGERQLQKIER
113-127	29	MGERQLQKIERWFVR
117-131	30	QLQKIERWFVRNPFF
121-135	31	IERWFVRNPFFAVTA
125-139	32	FVRNPFFAVTALTIA
129-143	33	PFFAVTALTIAYLVG
133-147	34	VTALTIAYLVGSNMT
137-151	35	TIAYLVGSNMTQRVV
141-155	36	LVGSNMTQRVVIALL
145-159	37	NMTQRVVIALLVLAV
149-163	38	RVVIALLVLAVGPAY
153-164	39	ALLVLAVGPAYS

Table 5.4.1-3 Peptides of YFV E protein.

aa position	Peptide No.	Sequence
1-15	1	AHCIGITDRDFIEGV
5-19	2	GITDRDFIEGVHGGT
9-23	3	RDFIEGVHGGTWVSA
13-27	4	EGVHGGTWVSATLEQ
17-31	5	GGTWVSATLEQDKCV
21-35	6	VSATLEQDKCVTVMA
25-39	7	LEQDKCVTVMAPDKP
29-43	8	KCVTVMAPDKPSLDI
33-47	9	VMAPDKPSLDISLET
37-51	10	DKPSLDISLETVAID
41-55	11	LDISLETVAIDRPAE
45-59	12	LETVAIDRPAEVRKV
49-63	13	AIDRPAEVRKVCYNA
53-67	14	PAEVRKVCYNAVLTH
57-71	15	RKVCYNAVLTHVKIN
61-75	16	YNAVLTHVKINDKCP
65-79	17	LTHVKINDKCPSTGE
69-83	18	KINDKCPSTGEAHLA
73-87	19	KCPSTGEAHLAEENE
77-91	20	TGEAHLAEENEGDNA
81-95	21	HLAEENEGDNACKRT
85-99	22	ENEGDNACKRTYSDR
89-103	23	DNACKRTYSDRGWGN
93-107	24	KRTYSDRGWGNGCGL
97-111	25	SDRGWGNGCGLFGKG
101-115	26	WGNGCGLFGKGSIVA
105-119	27	CGLFGKGSIVACAKF
109-123	28	GKGSIVACAKFTCAK
113-127	29	IVACAKFTCAKSMSL
117-131	30	AKFTCAKSMSLFEVD
121-135	31	CAKSMSLFEVDQTKI
125-139	32	MSLFEVDQTKIQYVI
129-143	33	EVDQTKIQYVIRAQL
133-147	34	TKIQYVIRAQLHVGA
137-151	35	YVIRAQLHVGAKQEN
141-155	36	AQLHVGAKQENWNTD
145-159	37	VGAKQENWNTDIKTL
149-163	38	QENWNTDIKTLKFDA
153-167	39	NTDIKTLKFDALSGS
157-171	40	KTLKFDALSGSQEVE
161-175	41	FDALSGSQEVEFIGY
165-179	42	SGSQEVEFIGYGKAT
169-183	43	EVEFIGYGKATLECQ
173-187	44	IGYGKATLECQVQTA
177-191	45	KATLECQVQTAVDFG
181-195	46	ECQVQTAVDFGNSYI
185-199	47	QTAVDFGNSYIAEME
189-203	48	DFGNSYIAEMETESW
193-207	49	SYIAEMETESWIVDR
197-211	50	EMETESWIVDRQWAQ
201-215	51	ESWIVDRQWAQDLTL
205-219	52	VDRQWAQDLTLPWQS
209-223	53	WAQDLTLPWQSGSGG
213-227	54	LTLPWQSGSGGVWRE
217-231	55	WQSGSGGVWREMHHL
221-235	56	SGGVWREMHHLVEFE
225-239	57	WREMHHLVEFEPPHA
229-243	58	HHLVEFEPPHAATIR
233-247	59	EFEPPHAATIRVLAL
237-251	60	PHAATIRVLALGNQE
241-255	61	TIRVLALGNQEGSLK

aa position	Peptide No.	Sequence
245-259	62	LALGNQEGSLKTALT
249-263	63	NQEGSLKTALTGAMR
253-267	64	SLKTALTGAMRVTKD
257-271	65	ALTGAMRVTKDTNDN
261-275	66	AMRVTKDTNDNNLYK
265-279	67	TKDTNDNNLYKLHGG
269-283	68	NDNNLYKLHGGHVSC
273-287	69	LYKLHGGHVSCRVKL
277-291	70	HGGHVSCRVKLSALT
281-295	71	VSCRVKLSALTLKGT
285-299	72	VKLSALTLKGTSYKI
289-303	73	ALTLKGTSYKICTDK
293-307	74	KGTSYKICTDKMFFV
297-311	75	YKICTDKMFFVKNPT
301-315	76	TDKMFFVKNPTDTGH
305-319	77	FFVKNPTDTGHGTVV
309-323	78	NPTDTGHGTVVMQVK
313-327	79	TGHGTVVMQVKVSKG
317-331	80	TVVMQVKVSKGAPCR
321-335	81	QVKVSKGAPCRIPVI
325-339	82	SKGAPCRIPVIVADD
329-343	83	PCRIPVIVADDLTAA
333-347	84	PVIVADDLTAAINKG
337-351	85	ADDLTAAINKGILVT
341-355	86	TAAINKGILVTVNPI
345-359	87	NKGILVTVNPIASTN
349-363	88	LVTVNPIASTNDDEV
353-367	89	NPIASTNDDEVLIEV
357-371	90	STNDDEVLIEVNPPF
361-375	91	DEVLIEVNPPFGDSY
365-379	92	IEVNPPFGDSYIIVG
369-383	93	PPFGDSYIIVGRGDS
373-387	94	DSYIIVGRGDSRLTY
377-391	95	IVGRGDSRLTYQWHK
381-395	96	GDSRLTYQWHKEGSS
385-399	97	LTYQWHKEGSSIGKL
389-403	98	WHKEGSSIGKLFTQT
393-407	99	GSSIGKLFTQTMKGV
397-411	100	GKLFTQTMKGVERLA
401-415	101	TQTMKGVERLAVMGD
405-419	102	KGVERLAVMGDTAWD
409-423	103	RLAVMGDTAWDFSSA
413-427	104	MGDTAWDFSSAGGFF
417-431	105	AWDFSSAGGFFTSVG
421-435	106	SSAGGFFTSVGKGIH
425-439	107	GFFTSVGKGIHTVFG
429-443	108	SVGKGIHTVFGSAFQ
433-447	109	GIHTVFGSAFQGLFG
437-451	110	VFGSAFQGLFGGLNW
441-455	111	AFQGLFGGLNWITKV
445-459	112	LFGGLNWITKVIMGA
449-463	113	LNWITKVIMGAVLIW
453-467	114	TKVIMGAVLIWVGIN
457-471	115	MGAVLIWVGINTRNM
461-475	116	LIWVGINTRNMTMSM
465-479	117	GINTRNMTMSMSMIL
469-483	118	RNMTMSMSMILVGVI
473-487	119	MSMSMILVGVIMMFL
477-491	120	MILVGVIMMFLSLGV
481-493	121	GVIMMFLSLGVGA

A YFV C

Pool	I	II	III	IV	V	VI
VII	1	2	3	4	5	6
VIII	7	8	9	10	11	12
IX	13	14	15	16	17	18
X	19	20	21	22	23	24
XI	25	26	27	28		

B YFV prM/M

Pool	I	II	III	IV	V	VI	VII
VIII	1	2	3	4	5	6	7
IX	8	9	10	11	12	13	14
X	15	16	17	18	19	20	21
XI	22	23	24	25	26	27	28
XII	29	30	31	32	33	34	35
XIII	36	37	38	39			

C YFV E

Pool	I	II	III	IV	V	VI	VII	VIII	IX	X	XI
XII	1	2	3	4	5	6	7	8	9	10	11
XIII	12	13	14	15	16	17	18	19	20	21	22
XIV	23	24	25	26	27	28	29	30	31	32	33
XV	34	35	36	37	38	39	40	41	42	43	44
XVI	45	46	47	48	49	50	51	52	53	54	55
XVII	56	57	58	59	60	61	62	63	64	65	66
XVIII	67	68	69	70	71	72	73	74	75	76	77
XIX	78	79	80	81	82	83	84	85	86	87	88
XX	89	90	91	92	93	94	95	96	97	98	99
XXI	100	101	102	103	104	105	106	107	108	109	110
XXII	111	112	113	114	115	116	117	118	119	120	121

Fig. 5.4.1 Two-dimensional peptide pool matrices. Single peptides of YFV C (A), prM/M (B) and E (C) proteins were grouped into Matrix Pools (Roman numerals) by a two-dimensional matrix. Arabic numerals of the 15-mer single peptides were assigned according to the appearance within the amino acid sequence of the respective structural protein. Each peptide was present in 2 distinct Matrix Pools.

5.4.2. Tick-borne encephalitis virus peptides

For the assay control, we used 26, 40 and 122 15-mer peptides from JPT (Berlin, Germany) which overlap by 11 amino acids and cover the entire sequences of C, prM/M and E structural proteins from TBEV Neudoerfl (GI 27596775, GI 27596776 and GI 27596778; table 5.4.2). Purity of all peptides was >70% as determined by high performance liquid chromatography (HPLC).

Lyophilized TBEV peptides were dissolved, diluted and preserved as described for YFV. To determine the magnitude of CD4+ T cell responses to TBEV structural proteins, TBEV peptides were arranged into three Maxi Pools which cover the entire sequences of C, prM/M and E proteins.

Table 5.4.2-1 Peptides of TBEV C protein.

aa position	Peptide No.	Sequence
1-15	1	MVKKAILKGKGGGPP
5-19	2	AILKGKGGGPPRRVS
9-23	3	GKGGGPPRRVSKETA
13-27	4	GPPRRVSKETATKTR
17-31	5	RVSKETATKTRQPRV
21-35	6	ETATKTRQPRVQMPN
25-39	7	KTRQPRVQMPNGLVL
29-43	8	PRVQMPNGLVLMRMM
33-47	9	MPNGLVLMRMMGILW
37-51	10	LVLMRMMGILWHAVA
41-55	11	RMMGILWHAVAGTAR
45-59	12	ILWHAVAGTARNPVL
49-63	13	AVAGTARNPVLKAFW
53-67	14	TARNPVLKAFWNSVP
57-71	15	PVLKAFWNSVPLKQA
61-75	16	AFWNSVPLKQATAAL
65-79	17	SVPLKQATAALRKIK
69-83	18	KQATAALRKIKRTVS
73-87	19	AALRKIKRTVSALMV
77-91	20	KIKRTVSALMVGLQK
81-95	21	TVSALMVGLQKRGKR
85-99	22	LMVGLQKRGKRRSAT
89-103	23	LQKRGKRRSATDWMS
93-107	24	GKRRSATDWMSWLLV
97-111	25	SATDWMSWLLVITLL
101-112	26	WMSWLLVITLLG

Table 5.4.2-2 Peptides of TBEV prM/M protein.

aa position	Peptide No.	Sequence
1-15	1	MTLAATVRKERDGST
5-19	2	ATVRKERDGSTVIRA
9-23	3	KERDGSTVIRAEGKD
13-27	4	GSTVIRAEGKDAATQ
17-31	5	IRAEGKDAATQVRVE
21-35	6	GKDAATQVRVENGTC
25-39	7	ATQVRVENGTCVILA
29-43	8	RVENGTCVILATDMG
33-47	9	GTCVILATDMGSWCD
37-51	10	ILATDMGSWCDDSLS
41-55	11	DMGSWCDDSLSYECV
45-59	12	WCDDSLSYECVTIDQ
49-63	13	SLSYECVTIDQGEEP
53-67	14	ECVTIDQGEEPVDVD
57-71	15	IDQGEEPVDVDCFCR
61-75	16	EEPVDVDCFCRNVDG
65-79	17	DVDCFCRNVDGVYLE
69-83	18	FCRNVDGVYLEYGRC
73-87	19	VDGVYLEYGRCGKQE
77-91	20	YLEYGRCGKQEGSRT
81-95	21	GRCGKQEGSRTRRSV
85-99	22	KQEGSRTRRSVLIPS
89-103	23	SRTRRSVLIPSHAQG
93-107	24	RSVLIPSHAQGELTG
97-111	25	IPSHAQGELTGRGHK
101-115	26	AQGELTGRGHKWLEG
105-119	27	LTGRGHKWLEGDSLR
109-123	28	GHKWLEGDSLRTHLT
113-127	29	LEGDSLRTHLTRVEG
117-131	30	SLRTHLTRVEGWVWK
121-135	31	HLTRVEGWVWKNKLL
125-139	32	VEGWVWKNKLLALAM
129-143	33	VWKNKLLALAMVTVV
133-147	34	KLLALAMVTVVWLTL
137-151	35	LAMVTVVWLTLESVV
141-155	36	TVVWLTLESVVTRVA
145-159	37	LTLESVVTRVAVLVV
149-163	38	SVVTRVAVLVVLLCL
153-167	39	RVAVLVVLLCLAPVY
157-168	40	LVVLLCLAPVYA

Table 5.4.2-3 Peptides of TBEV E protein.

aa position	Peptide No.	Sequence
1-15	1	SRCTHLENRDFVTGT
5-19	2	HLENRDFVTGTQGTT
9-23	3	RDFVTGTQGTTRVTL
13-27	4	TGTQGTTRVTLVLEL
17-31	5	GTTRVTLVLELGGCV
21-35	6	VTLVLELGGCVTITA
25-39	7	LELGGCVTITAEGKP
29-43	8	GCVTITAEGKPSMDV
33-47	9	ITAEGKPSMDVWLDA
37-51	10	GKPSMDVWLDAIYQE
41-55	11	MDVWLDAIYQENPAK
45-59	12	LDAIYQENPAKTREY
49-63	13	YQENPAKTREYCLHA
53-67	14	PAKTREYCLHAKLSD
57-71	15	REYCLHAKLSDTKVA
61-75	16	LHAKLSDTKVAARCP
65-79	17	LSDTKVAARCPTMGP
69-83	18	KVAARCPTMGPATLA
73-87	19	RCPTMGPATLAEEHQ
77-91	20	MGPATLAEEHQGGTV
81-95	21	TLAEEHQGGTVCKRD
85-99	22	EHQGGTVCKRDQSDR
89-103	23	GTVCKRDQSDRGWGN
93-107	24	KRDQSDRGWGNHCGL
97-111	25	SDRGWGNHCGLFGKG
101-115	26	WGNHCGLFGKGSIVA
105-119	27	CGLFGKGSIVACVKA
109-123	28	GKGSIVACVKAACEA
113-127	29	IVACVKAACEAKKKA
117-131	30	VKAACEAKKKATGHV
121-135	31	CEAKKKATGHVYDAN
125-139	32	KKATGHVYDANKIVY
129-143	33	GHVYDANKIVYTVKV
133-147	34	DANKIVYTVKVEPHT
137-151	35	IVYTVKVEPHTGDYV
141-155	36	VKVEPHTGDYVAANE
145-159	37	PHTGDYVAANETHSG
149-163	38	DYVAANETHSGRKTA
153-167	39	ANETHSGRKTASFTI
157-171	40	HSGRKTASFTISSEK
161-175	41	KTASFTISSEKTILT
165-179	42	FTISSEKTILTMGEY
169-183	43	SEKTILTMGEYGDVS
173-187	44	ILTMGEYGDVSLLCR
177-191	45	GEYGDVSLLCRVASG
181-195	46	DVSLLCRVASGVDLA
185-199	47	LCRVASGVDLAQTVI
189-203	48	ASGVDLAQTVILELD
193-207	49	DLAQTVILELDKTVE
197-211	50	TVILELDKTVEHLPT
201-215	51	ELDKTVEHLPTAWQV
205-219	52	TVEHLPTAWQVHRDW
209-223	53	LPTAWQVHRDWFNDL
213-227	54	WQVHRDWFNDLALPW
217-231	55	RDWFNDLALPWKHEG
221-235	56	NDLALPWKHEGAQNW
225-239	57	LPWKHEGAQNWNNAE
229-243	58	HEGAQNWNNAERLVE
233-247	59	QNWNNAERLVEFGAP
237-251	60	NAERLVEFGAPHAVK
241-255	61	LVEFGAPHAVKMDVY
245-259	62	GAPHAVKMDVYNLGD
249-263	63	AVKMDVYNLGDQTGV
253-267	64	DVYNLGDQTGVLLKA
257-271	65	LGDQTGVLLKALAGV
261-275	66	TGVLLKALAGVPVAH
265-279	67	LKALAGVPVAHIEGT
269-283	68	AGVPVAHIEGTKYHL
273-287	69	VAHIEGTKYHLKSGH
277-291	70	EGTKYHLKSGHVTCE
281-295	71	YHLKSGHVTCEVGLE
285-299	72	SGHVTCEVGLEKLKM
289-303	73	TCEVGLEKLKMKGLT
293-307	74	GLEKLKMKGLTYTMC
297-311	75	LKMKGLTYTMCDKTK
301-315	76	GLTYTMCDKTKFTWK
305-319	77	TMCDKTKFTWKRAPT
309-323	78	KTKFTWKRAPTDSGH
313-327	79	TWKRAPTDSGHDTVV
317-331	80	APTDSGHDTVVMEVT
321-335	81	SGHDTVVMEVTFSGT
325-339	82	TVVMEVTFSGTKPCR
329-343	83	EVTFSGTKPCRIPVR
333-347	84	SGTKPCRIPVRAVAH
337-351	85	PCRIPVRAVAHGSPD
341-355	86	PVRAVAHGSPDVNVA
345-359	87	VAHGSPDVNVAMLIT
349-363	88	SPDVNVAMLITPNPT
353-367	89	NVAMLITPNPTIENN
357-371	90	LITPNPTIENNGGGF
361-375	91	NPTIENNGGGFIEMQ
365-379	92	ENNGGGFIEMQLPPG
369-383	93	GGFIEMQLPPGDNII
373-387	94	EMQLPPGDNIIYVGE
377-391	95	PPGDNIIYVGELSHQ
381-395	96	NIIYVGELSHQWFQK
385-399	97	VGELSHQWFQKGSSI
389-403	98	SHQWFQKGSSIGRVF
393-407	99	FQKGSSIGRVFQKTK
397-411	100	SSIGRVFQKTKKGIE
401-415	101	RVFQKTKKGIERLTV
405-419	102	KTKKGIERLTVIGEH
409-423	103	GIERLTVIGEHAWDF
413-427	104	LTVIGEHAWDFGSAG
417-431	105	GEHAWDFGSAGGFLS
421-435	106	WDFGSAGGFLSSIGK
425-439	107	SAGGFLSSIGKAVHT
429-443	108	FLSSIGKAVHTVLGG
433-447	109	IGKAVHTVLGGAFNS
437-451	110	VHTVLGGAFNSIFGG
441-455	111	LGGAFNSIFGGVGFL
445-459	112	FNSIFGGVGFLPKLL
449-463	113	FGGVGFLPKLLLGVA
453-467	114	GFLPKLLLGVALAWL
457-471	115	KLLLGVALAWLGLNM
461-475	116	GVALAWLGLNMRNPT
465-479	117	AWLGLNMRNPTMSMS
469-483	118	LNMRNPTMSMSFLLA
473-487	119	NPTMSMSFLLAGGLV
477-491	120	SMSFLLAGGLVLAMT
481-495	121	LLAGGLVLAMTLGVG
485-496	122	GLVLAMTLGVGA

5.5. IL-2 ELISPOT assay

The IL-2 ELISPOT assay (Mabtech) was conducted according to manufacturer´s instructions. In short, polyvinylidene difluoride (PVDF)-ELISPOT plates (MSIPS4W10, Merck-Millipore) were treated with 70% ethanol for 30 minutes prior to coating with 1 µg anti-IL-2 antibody (3445-3-1000, Mabtech). Plates were blocked with RPMI 1640 medium (Sigma) containing 10% human serum (PAA), 1% penicillin/streptomycin/glutamine (Gibco) and 1% nonessential amino acids (Sigma) for one to three hours at 37°C and 5% CO_2. Plates were washed with phosphate buffered saline (PBS). Subsequently, 50 µl AIM V medium (Gibco) and 2 x 10^5 CD8-depleted PBMCs in 100 µl AIM V medium were added into each well. Cells were stimulated with 50 µl of either peptide pools or single peptides at a final concentration of 2 µg of each peptide/ml. As positive and negative controls, phytohemagglutinin (PHA, Sigma) at a final concentration of 0.5 µg/ml and AIM V medium were used. PBMCs were incubated approximately 48 hours at 37°C and 5% CO_2. Afterwards, plates were washed twice with PBS containing 0.05% Tween 20 and twice with PBS. Detection of immobilized IL-2 was performed at room temperature with 0.05 µg biotin-conjugated antibody (3445-6-250, Mabtech) for two hours, streptavidin-coupled alkaline phosphatase (ALP; 1:1000, 3310-10, Mabtech) for 45 minutes and 5-bromo-4-chloro-3-indolylphosphate/nitroblue tetrazolium (BCIP/NBT; B5655, Sigma) for 15 minutes. Plates were dried overnight and developed spots were analyzed using a Bio-Sys Bioreader 5000 Pro-S/BR177 and Bioreader software, generation 10.

As described previously (79, 95, 107), data was computed as IL-2 spot forming cells (SFCs)/1x10^6 CD8-depleted PBMCs after subtraction of the negative control (mean spot number from three to four unstimulated wells). The response to a single peptide was defined positive if corresponding Maxi Pool, Matrix Pool and single peptide assays yielded >20 SFCs/1 x 10^6 CD8-depleted PBMCs. The number of SFCs in 10 flavivirus-naïve individuals after stimulation with Maxi Pools C, prM/M and E did not exceed 20 SFCs/1 x 10^6 CD8-depleted PBMCs. Across this control group, mean SFCs plus 3 standard deviations did not exceed 20 SFCs/1 x 10^6 CD8-depleted PBMCs. Replicate tests using single peptides were not possible due to limited PBMC samples.

5.6. Assay controls

5.6.1. Cell viability and CD8-depletion efficiency

Prior to ELISPOT assays, viability of PBMCs and efficiency of CD8 depletion was monitored for each sample by flow cytometry using anti-CD3-phycoerythrin (PE), anti-CD8-allophycocyanin (APC), anti-CD4-PacificBlue™ and 7-aminoactinomycin D (7-AAD) (all purchased from BD Bioscience). After depletion, PBMC samples contained usually less than 1% CD3+/CD8+/CD4- T cells (Fig. 5.5.1).

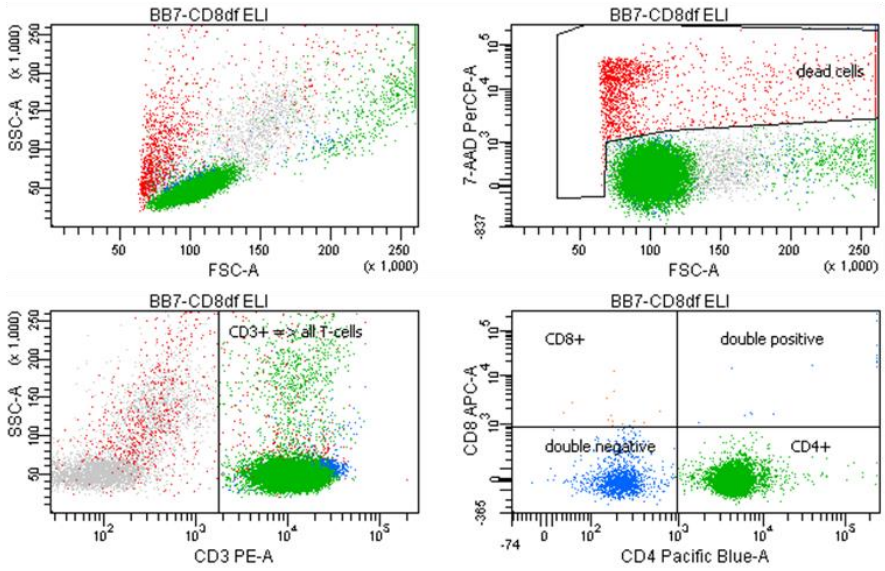

Fig. 5.6.1 Control of CD8-depletion efficiency. Depletion of CD8+ T cells from all IL-2 ELISPOT tested samples was assessed using flow cytometry. The CD8-depleted PBMCs were gated on lymphocytes (small, non-granulated cell population; upper left panel). Dead cells (i.e. 7AAD-positive cells) were gated out (upper right panel). Viable lymphocytes were gated on CD3-positive cells (lower left panel). Subsequently, the percentages of CD8+ T cells were assessed (lower right panel).

5.6.2. ELISPOT controls

To determine individual CD4+ T cell responses to YFV structural proteins, we included the following controls in each ELISPOT assay (Fig. 5.5.2). To validate the specificity of antibodies used for IL-2 detection, we also evaluated blank wells (cell-free). In order to assess the basal level of T cell activation, we employed a negative control (unstimulated cells). Overall, SFCs in unstimulated wells were usually infrequent which highlights excellent PBMC sample quality and cell culture conditions. To assess the presence of IL-2 producing CD4+ T cells, we stimulated one well per ELISPOT with phytohemagglutinin (PHA). Representative images of these controls and autologous PBMCs stimulated with peptide pools covering the entire sequences of YFV C, prM/M and E proteins are shown in Fig. 5.5.2.

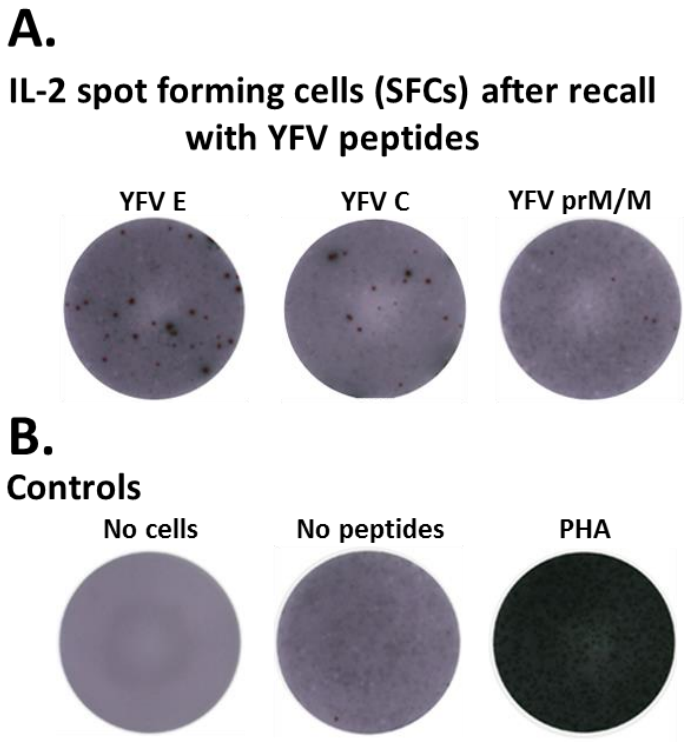

Fig. 5.6.2 YFV-specific restimulation of CD4+ T cells. Representative images of an individual IL-2 ELISPOT. Equal cell numbers ($2x10^5$ CD8-depleted PBMCs/well) were applied in (A) and (B, middle and right panel). Activated, IL-2 producing, CD4+ T cells appear as spot forming cells (SFCs) on the membrane of the ELISPOT plate. (A) SFCs of PBMCs stimulated with peptide pools covering the entire sequences of YFV structural proteins C, prM/M and E. (B) Images of cell-free, unstimulated and PHA-stimulated wells.

5.6.3. Assay control

To validate long-term robustness of our assay, we determined CD4+ T cell responses against TBEV structural proteins C, prM/M and E of one TBEV vaccinated blood donor in parallel with each YFV ELISPOT (Fig. 5.5.3). Statistical evaluation revealed a coefficient of variation between 13% (C) and 10% (E) and showed no significant trend over time, indicating robust study results.

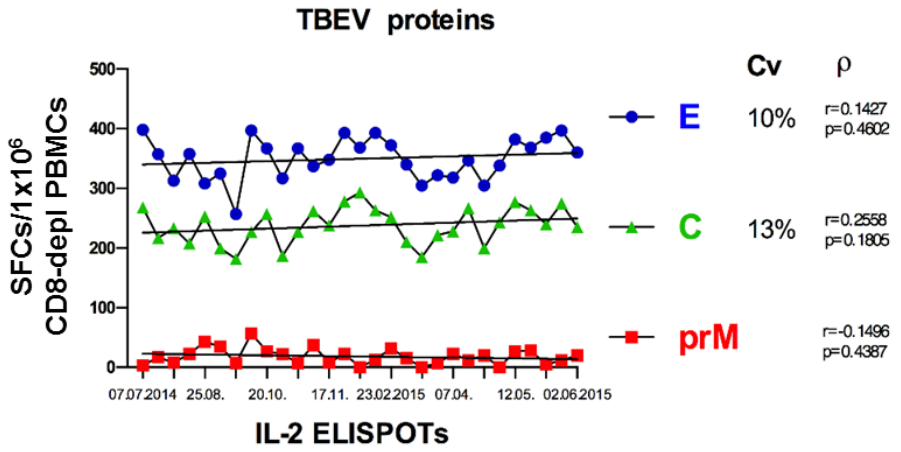

Fig. 5.6.3 Assay control over a 12-month period. Magnitude of CD4+ T cell responses from one TBEV vaccinated blood donor against TBEV structural proteins C, prM/M and E. Results of 29 IL-2 ELISPOTs are shown. Results are given as spot forming cells (SFCs)/1x10^6 CD8-depleted PBMCs. The statistical analysis is shown on the right (coefficient of variation and Spearman correlation).

5.7. Neutralization assays

5.7.1. TBEV neutralization test

TBEV neutralization tests (NTs) were conducted as described previously (117). Briefly, neutralization assays were carried out in baby hamster kidney cells (ATCC BHK-21). Two-fold serial dilutions of heat-inactivated serum samples (duplicates) were incubated with 25 plaque-forming units (PFU) TBE virus strain Neudoerfl for 1 h at 37 °C. Cells were added and incubation was continued for 3 days. Afterwards, presence of virus in the supernatant was assessed by ELISA. The virus neutralization titer was defined as the reciprocal of the serum sample dilution that gave a 90% reduction in the absorbance readout in the assay compared to the control without antibody. NT titers ≥10 were considered positive.

5.7.2. YFV neutralization test

YFV neutralization tests (NTs) were carried out in baby hamster kidney cells (ATCC BHK-21) using the Yellow fever virus strain 17D (126). Two-fold serial dilutions of heat-inactivated serum samples (duplicates) were incubated with 50-100 TCID50 virus for 1 h at 37°C. Cells were then added and incubation was continued for 3 days. The presence of virus in the supernatant was assessed by the occurrence of cytopathic effects. NT titers ≥20 were considered positive.

5.8. Structural analysis

The immunodominant YFV-17D epitopes were assigned to crystallographic structures of KUNV C protein (PDB: 1SFK) (26) and TBEV soluble E (sE) protein which lacks stem and transmembrane domains (PDB: 1SVB) (94) since no crystallographic data was available for YFV structural proteins at the time of study completion.

Allocation of dominant epitopes was conducted by use of PyMOL software. For high fidelity epitope assignment, amino acid sequences of seven flaviviruses (YFV [P03314], TBEV[GI 27596775 and GI 27596778], DENV2 [P29990], DENV3 [P27915], WNV [P06935], KUNV [P14335], JEV [P27395]) were aligned using Promals software (87).

5.9. HLA genotyping

Genotyping of HLA-DRB1/3/4/5 and HLA-DQB1 was carried out by nucleotide sequencing of exon 2. HLA-DPB1 alleles were determined by nucleotide sequencing of exon 2 and 3 (30, 60).

In short, amplification products were purified by polyethylene glycol (PEG) precipitation and directly sequenced. To this end, cycle sequencing with Big Dye Terminator chemistry on an ABI 3100 capillary sequencing device was performed. Sequences were analyzed using GenDX SBT Engine software (GenDX, Utrecht, the Netherlands). Subsequent comparison with the ImMunoGeneTics (IMGT)/HLA database enabled the assignment of individual HLA-alleles.

5.10. MHC class-II binding prediction using IEDB

Binding predictions for YFV peptides and human MHC-II molecules were made in August 2015. For this purpose, we used the Immune Epitope Database (IEDB) MHC-II binding prediction tool with settings “IEDB recommended” and “HLA allele reference set” (33, 39, 127, 128).

Amino acid sequences of the YFV-17D structural proteins C and E (P03314) were screened separately against a HLA reference set representing 99% population coverage (HLA-DRB1*01:01, HLA-DRB1*03:01, HLA-DRB1*04:01, HLA-DRB1*04:05, HLA-DRB1*07:01, HLA-DRB1*08:02, HLA-DRB1*09:01, HLA-DRB1*11:01, HLA-DRB1*12:01, HLA-DRB1*13:02, HLA-DRB1*15:01, HLA-DRB3*01:01, HLA-DRB3*02:02, HLA-DRB4*01:01, HLA-DRB5*01:01, HLA-DQA1*05:01/DQB1*02:01, HLA-DQA1*05:01/DQB1*03:01, HLA-DQA1*03:01/DQB1*03:02, HLA-DQA1*04:01/DQB1*04:02, HLA-DQA1*01:01/DQB1*05:01, HLA-DQA1*01:02/DQB1*06:02, HLA-DPA1*02:01/DPB1*01:01, HLA-DPA1*01:03/DPB1*02:01, HLA-DPA1*01/DPB1*04:01, HLA-DPA1*03:01/DPB1*04:02, HLA-DPA1*02:01/DPB1*05:01, HLA-DPA1*02:01/DPB1*14:01).

Peptides with the highest predicted affinities for certain HLA alleles (i.e. IEDB percentile rank score of 10 or lower) were analyzed in relation to the experimental epitope data.

5.11. Statistical analysis

All statistical tests were conducted with GraphPad Prism (version 5).

Magnitude of CD4+ T cell responses in assay control samples was evaluated using linear regressions.

To compare the magnitude of CD4+ T cell responses to C, prM/M and E proteins in YFV-17D vaccinated individuals, a nonparametric Kruskal-Wallis test was used.

A fisher´s exact or chi-square test was used to identify the peptides that most frequently induced CD4+ T cell responses within the yellow fever vaccinated study cohort.

Spearman correlations were used to correlate the following parameters: C and E protein-specific T cell responses, neutralizing antibody titers and demographic characteristics.

References

1. 1984. Yellow-Fever Vaccine - Recommendations of the Immunization-Practices-Advisory-Committee. Annals of Internal Medicine **100:**540-542.
2. **Abbas, A. K., A. H. Lichtman, and S. Pillai.** 2012. Activation of T Lymphocytes, p. 203-224, Cellular and Molecular Immunology, 7th ed. Saunders, Elsevier, Philadelphia.
3. **Abbas, A. K., A. H. Lichtman, and S. Pillai.** 2007. The major histocompatibility complex, p. 97-111, Cellular and Molecular Immunology, 6th ed. Saunders, Elsevier, Philadelphia.
4. **Abbas, A. K., A. H. Lichtman, and S. Pillai.** 2012. Major Histocompatibility Complex Molecules and Antigen Presentation to T Lymphocytes, p. 109-138, Cellular and Molecular Immunology, 7th ed. Saunders, Elsevier, Philadelphia.
5. **Aberle, J. H., K. Stiasny, M. Kundi, and F. X. Heinz.** 2013. Mechanistic insights into the impairment of memory B cells and antibody production in the elderly. Age (Dordr) **35:**371-81.
6. **Akondy, R. S., N. D. Monson, J. D. Miller, S. Edupuganti, D. Teuwen, H. Wu, F. Quyyumi, S. Garg, J. D. Altman, C. Del Rio, H. L. Keyserling, A. Ploss, C. M. Rice, W. A. Orenstein, M. J. Mulligan, and R. Ahmed.** 2009. The Yellow Fever Virus Vaccine Induces a Broad and Polyfunctional Human Memory CD8(+) T Cell Response. Journal of Immunology **183:**7919-7930.
7. **Anthony, D. D., and P. V. Lehmann.** 2003. T-cell epitope mapping using the ELISPOT approach. Methods **29:**260-269.
8. **Assarsson, E., J. Sidney, C. Oseroff, V. Pasquetto, H. H. Bui, N. Frahm, C. Brander, B. Peters, H. Grey, and A. Sette.** 2007. A quantitative analysis of the variables affecting the repertoire of T cell specificities recognized after vaccinia virus infection. Journal of Immunology **178:**7890-7901.
9. **Aw, D., A. B. Silva, and D. B. Palmer.** 2007. Immunosenescence: emerging challenges for an ageing population. Immunology **120:**435-46.
10. **Bandyopadhyay, A., L. Arneson, C. Beeson, and A. J. Sant.** 2008. The relative energetic contributions of dominant P1 pocket versus hydrogen bonding interactions to peptide : class II stability: Implications for the mechanism of DM function. Molecular Immunology **45:**1248-1257.
11. **Barrett, A. D. T., and D. E. Teuwen.** 2009. Yellow fever vaccine - how does it work and why do rare cases of serious adverse events take place? Current Opinion in Immunology **21:**308-313.
12. **Bassi, M. R., M. Kongsgaard, M. A. Steffensen, C. Fenger, M. Rasmussen, K. Skjodt, B. Finsen, A. Stryhn, S. Buus, J. P. Christensen, and A. R. Thomsen.** 2015. CD8(+) T Cells Complement Antibodies in Protecting against Yellow Fever Virus. Journal of Immunology **194:**1141-1153.
13. **Belmusto-Worn, V. E., J. L. Sanchez, K. McCarthy, R. Nichols, C. T. Bautista, A. J. Magill, G. Pastor-Cauna, C. Echevarria, V. A. Laguna-Torres, B. K. Samame, M. E. Baldeon, J. P. Burans, J. G. Olson, P. Bedford, S. Kitchener, and T. P. Monath.** 2005. Randomized, double-blind, phase III, pivotal field trial of the comparative immunogenicity, safety, and tolerability of two yellow fever 17D vaccines (ARILVAX (TM) and YF-VAX (R)) in healthy infants and children in Peru. American Journal of Tropical Medicine and Hygiene **72:**189-197.
14. **Bihl, F., N. Frahm, L. Di Giammarino, J. Sidney, M. John, K. Yusim, T. Woodberry, K. Sango, H. S. Hewitt, L. Henry, C. H. Linde, J. V. Chisholm, 3rd, T. M. Zaman, E. Pae, S. Mallal, B. D. Walker, A. Sette, B. T. Korber, D. Heckerman, and C. Brander.** 2006. Impact of HLA-B alleles, epitope binding affinity, functional avidity, and viral coinfection on the immunodominance of virus-specific CTL responses. J Immunol **176:**4094-101.
15. **Bird, P. I., J. A. Trapani, and J. A. Villadangos.** 2009. Endolysosomal proteases and their inhibitors in immunity. Nat Rev Immunol **9:**871-82.
16. **Blum, J. S., P. A. Wearsch, and P. Cresswell.** 2013. Pathways of antigen processing. Annu Rev Immunol **31:**443-73.

17. **Bressanelli, S., K. Stiasny, S. L. Allison, E. A. Stura, S. Duquerroy, J. Lescar, F. X. Heinz, and F. A. Rey.** 2004. Structure of a flavivirus envelope glycoprotein in its low-pH-induced membrane fusion conformation. Embo Journal **23:**728-738.
18. **Brien, J. D., J. L. Uhrlaub, and J. Nikolich-Zugich.** 2008. West Nile virus-specific CD4 T cells exhibit direct antiviral cytokine secretion and cytotoxicity and are sufficient for antiviral protection. J Immunol **181:**8568-75.
19. **Brown, S. A., J. Stambas, X. Zhan, K. S. Slobod, C. Coleclough, A. Zirkel, S. Surman, S. W. White, P. C. Doherty, and J. L. Hurwitz.** 2003. Clustering of Th cell epitopes on exposed regions of HIV envelope despite defects in antibody activity. J Immunol **171:**4140-8.
20. **Bryson, C. J., T. D. Jones, and M. P. Baker.** 2010. Prediction of immunogenicity of therapeutic proteins: validity of computational tools. BioDrugs **24:**1-8.
21. **Chaves, F. A., A. H. Lee, J. L. Nayak, K. A. Richards, and A. J. Sant.** 2012. The utility and limitations of current Web-available algorithms to predict peptides recognized by CD4 T cells in response to pathogen infection. J Immunol **188:**4235-48.
22. **Chianese-Bullock, K. A., H. I. Russell, C. Moller, W. Gerhard, J. J. Monaco, and L. C. Eisenlohr.** 1998. Antigen processing of two H2-IEd-restricted epitopes is differentially influenced by the structural changes in a viral glycoprotein. Journal of Immunology **161:**1599-1607.
23. **Chu, J. J., R. Rajamanonmani, J. Li, R. Bhuvanakantham, J. Lescar, and M. L. Ng.** 2005. Inhibition of West Nile virus entry by using a recombinant domain III from the envelope glycoprotein. J Gen Virol **86:**405-12.
24. **Crill, W. D., and J. T. Roehrig.** 2001. Monoclonal antibodies that bind to domain III of dengue virus E glycoprotein are the most efficient blockers of virus adsorption to Vero cells. J Virol **75:**7769-73.
25. **De Filette, M., S. Soehle, S. Ulbert, J. Richner, M. S. Diamond, A. Sinigaglia, L. Barzon, S. Roels, J. Lisziewicz, O. Lorincz, and N. N. Sanders.** 2014. Vaccination of Mice Using the West Nile Virus E-Protein in a DNA Prime-Protein Boost Strategy Stimulates Cell-Mediated Immunity and Protects Mice against a Lethal Challenge. Plos One **9**.
26. **Dokland, T., M. Walsh, J. M. Mackenzie, A. A. Khromykh, K. H. Ee, and S. Wang.** 2004. West Nile virus core protein; tetramer structure and ribbon formation. Structure **12:**1157-63.
27. **EBI.** 2016. http://www.ebi.ac.uk/ipd/imgt/hla/stats.html.
28. **Eisenlohr, L. C., N. Luckashenak, S. Apcher, M. A. Miller, and G. Sinnathamby.** 2011. Beyond the classical: influenza virus and the elucidation of alternative MHC class II-restricted antigen processing pathways. Immunol Res **51:**237-48.
29. **Fischer, A., S. Nash, P. C. Beverley, and M. Feldmann.** 1982. An influenza virus matrix protein-specific human T cell line with helper activity for in vitro anti-hemagglutinin antibody production. Eur J Immunol **12:**844-9.
30. **Fischer, G. F., I. Fae, M. Petrasek, H. Haas, and W. R. Mayr.** 1995. An Hla-Dr11 Variant (Hla-Drb1(Asterisk)1115) Segregating in a Family of Turkish Origin. Tissue Antigens **45:**143-144.
31. **Gardner, C. L., and K. D. Ryman.** 2010. Yellow Fever: A Reemerging Threat. Clinics in Laboratory Medicine **30:**237-+.
32. **Gelder, C., M. Davenport, M. Barnardo, T. Bourne, J. Lamb, B. Askonas, A. Hill, and K. Welsh.** 1998. Six unrelated HLA-DR-matched adults recognize identical CD4(+) T cell epitopes from influenza A haemagglutinin that are not simply peptides with high HLA-DR binding affinities. International Immunology **10:**211-222.
33. **Greenbaum, J., J. Sidney, J. Chung, C. Brander, B. Peters, and A. Sette.** 2011. Functional classification of class II human leukocyte antigen (HLA) molecules reveals seven different supertypes and a surprising degree of repertoire sharing across supertypes. Immunogenetics **63:**325-35.
34. **Guce, A. I., S. E. Mortimer, T. Yoon, C. A. Painter, W. Jiang, E. D. Mellins, and L. J. Stern.** 2013. HLA-DO acts as a substrate mimic to inhibit HLA-DM by a competitive mechanism. Nat Struct Mol Biol **20:**90-8.

35. **Haynes, N. M.** 2008. Follicular associated T cells and their B-cell helper qualities. Tissue Antigens **71:**97-104.
36. **Heinz, F. X., H. Holzmann, A. Essl, and M. Kundi.** 2007. Field effectiveness of vaccination against tick-borne encephalitis. Vaccine **25:**7559-67.
37. **Heinz, F. X., and K. Stiasny.** 2012. Flaviviruses and flavivirus vaccines. Vaccine **30:**4301-6.
38. **Hughes, H. R., W. D. Crill, B. S. Davis, and G. J. J. Chang.** 2012. A West Nile virus CD4 T cell epitope improves the immunogenicity of dengue virus serotype 2 vaccines. Virology **424:**129-137.
39. **IEDB.** 2016. http://www.iedb.org/.
40. **James, E. A., R. E. LaFond, T. J. Gates, D. T. Mai, U. Malhotra, and W. W. Kwok.** 2013. Yellow fever vaccination elicits broad functional CD4+ T cell responses that recognize structural and nonstructural proteins. J Virol **87:**12794-804.
41. **Jenkins, M. K., and J. J. Moon.** 2012. The Role of Naive T Cell Precursor Frequency and Recruitment in Dictating Immune Response Magnitude. Journal of Immunology **188:**4135-4140.
42. **Jentes, E. S., G. Poumerol, M. D. Gershman, D. R. Hill, J. Lemarchand, R. F. Lewis, J. E. Staples, O. Tomori, A. Wilder-Smith, T. P. Monath, and I. W. W. G. Geographi.** 2011. The revised global yellow fever risk map and recommendations for vaccination, 2010: consensus of the Informal WHO Working Group on Geographic Risk for Yellow Fever. Lancet Infectious Diseases **11:**622-632.
43. **Junjhon, J., T. J. Edwards, U. Utaipat, V. D. Bowman, H. A. Holdaway, W. Zhang, P. Keelapang, C. Puttikhunt, R. Perera, P. R. Chipman, W. Kasinrerk, P. Malasit, R. J. Kuhn, and N. Sittisombut.** 2010. Influence of pr-M Cleavage on the Heterogeneity of Extracellular Dengue Virus Particles. Journal of Virology **84:**8353-8358.
44. **Kanai, R., K. Kar, K. Anthony, L. H. Gould, M. Ledizet, E. Fikrig, W. A. Marasco, R. A. Koski, and Y. Modis.** 2006. Crystal structure of west nile virus envelope glycoprotein reveals viral surface epitopes. J Virol **80:**11000-8.
45. **Kiermayr, S., R. M. Kofler, C. W. Mandl, P. Messner, and F. X. Heinz.** 2004. Isolation of capsid protein dimers from the tick-borne encephalitis flavivirus and in vitro assembly of capsid-like particles. Journal of Virology **78:**8078-8084.
46. **Kim, A., I. Z. Hartman, B. Poore, T. Boronina, R. N. Cole, N. Song, M. T. Ciudad, R. R. Caspi, D. Jaraquemada, and S. Sadegh-Nasseri.** 2014. Divergent paths for the selection of immunodominant epitopes from distinct antigenic sources. Nature Communications **5**.
47. **Kim, A., and S. Sadegh-Nasseri.** 2015. Determinants of immunodominance for CD4 T cells. Current Opinion in Immunology **34:**9-15.
48. **Kostyuchenko, V. A., Q. Zhang, J. L. Tan, T. S. Ng, and S. M. Lok.** 2013. Immature and Mature Dengue Serotype 1 Virus Structures Provide Insight into the Maturation Process. Journal of Virology **87:**7700-7707.
49. **Landry, S. J.** 2008. Three-dimensional structure determines the pattern of CD4(+) T-cell epitope dominance in influenza virus hemagglutinin. Journal of Virology **82:**1238-1248.
50. **Lang, J., J. Zuckerman, P. Clarke, P. Barrett, C. Kirkpatrick, and C. Blondeau.** 1999. Comparison of the immunogenicity and safety of two 17D yellow fever vaccines. American Journal of Tropical Medicine and Hygiene **60:**1045-1050.
51. **Lazarski, C. A., F. A. Chaves, S. A. Jenks, S. Wu, K. A. Richards, J. M. Weaver, and A. J. Sant.** 2005. The kinetic stability of MHC class II:peptide complexes is a key parameter that dictates immunodominance. Immunity **23:**29-40.
52. **Li, L., S. M. Lok, I. M. Yu, Y. Zhang, R. J. Kuhn, J. Chen, and M. G. Rossmann.** 2008. The flavivirus precursor membrane-envelope protein complex: structure and maturation. Science **319:**1830-4.
53. **Li, T. F., N. K. Steede, H. N. P. Nguyen, L. C. Freytag, J. B. McLachlan, R. R. Mettu, J. E. Robinson, and S. J. Landry.** 2014. Comprehensive Analysis of Contributions from Protein Conformational Stability and Major Histocompatibility Complex Class II-Peptide Binding

Affinity to CD4(+) Epitope Immunogenicity in HIV-1 Envelope Glycoprotein. Journal of Virology **88:**9605-9615.

54. **Liao, W. W., and J. W. Arthur.** 2011. Predicting peptide binding to Major Histocompatibility Complex molecules. Autoimmun Rev **10:**469-73.
55. **Lindenbach, B. D., C. L. Murray, H. J. Thiel, and C. M. Rice.** 2013. Flaviviridae, p. 712-746. *In* D. M. Knipe, P. M. Howley, J. I. Cohen, D. E. Griffin, R. A. Lamb, M. A. Martin, V. R. Racaniello, and B. Roizman (ed.), Fields Virology, 6 ed. Lippincott. Williams & Wilkins., Philadelphia.
56. **Lindsey, N. P., B. A. Schroeder, E. R. Miller, M. M. Braun, A. F. Hinckley, N. Marano, B. A. Slade, E. D. Barnett, G. W. Brunette, K. Horan, J. E. Staples, P. E. Kozarsky, and E. B. Hayes.** 2008. Adverse event reports following yellow fever vaccination. Vaccine **26:**6077-6082.
57. **Linton, P. J., and K. Dorshkind.** 2004. Age-related changes in lymphocyte development and function. Nat Immunol **5:**133-9.
58. **Litjens, N. H., M. Huisman, D. Hijdra, B. M. Lambrecht, K. J. Stittelaar, and M. G. Betjes.** 2008. IL-2 producing memory CD4+ T lymphocytes are closely associated with the generation of IgG-secreting plasma cells. J Immunol **181:**3665-73.
59. **Luca, V. C., J. AbiMansour, C. A. Nelson, and D. H. Fremont.** 2012. Crystal structure of the Japanese encephalitis virus envelope protein. J Virol **86:**2337-46.
60. **Ludajic, K., I. Fae, and G. F. Fischer.** 2006. Characterization of a new HLA-DPB1 allele, DPB1*010103. Tissue Antigens **67:**255-256.
61. **Ma, L., C. T. Jones, T. D. Groesch, R. J. Kuhn, and C. B. Post.** 2004. Solution structure of dengue virus capsid protein reveals another fold. Proc Natl Acad Sci U S A **101:**3414-9.
62. **Maciel, M., Jr., S. N. Kellathur, P. Chikhlikar, R. Dhalia, J. Sidney, A. Sette, T. J. August, and E. T. Marques, Jr.** 2008. Comprehensive analysis of T cell epitope discovery strategies using 17DD yellow fever virus structural proteins and BALB/c (H2d) mice model. Virology **378:**105-17.
63. **Mason, R. A., N. M. Tauraso, R. O. Spertzel, and R. K. Ginn.** 1973. Yellow fever vaccine: direct challenge of monkeys given graded doses of 17D vaccine. Appl Microbiol **25:**539-44.
64. **Mellins, E. D., and L. J. Stern.** 2014. HLA-DM and HLA-DO, key regulators of MHC-II processing and presentation. Current Opinion in Immunology **26:**115-122.
65. **Milich, D. R., A. McLachlan, G. B. Thornton, and J. L. Hughes.** 1987. Antibody production to the nucleocapsid and envelope of the hepatitis B virus primed by a single synthetic T cell site. Nature **329:**547-9.
66. **Miller, J. D., R. G. van der Most, R. S. Akondy, J. T. Glidewell, S. Albott, D. Masopust, K. Murali-Krishna, P. L. Mahar, S. Edupuganti, S. Lalor, S. Germon, C. Del Rio, M. J. Mulligan, S. I. Staprans, J. D. Altman, M. B. Feinberg, and R. Ahmed.** 2008. Human effector and memory CD8(+) T cell responses to smallpox and yellow fever vaccines. Immunity **28:**710-722.
67. **Miller, M. A., A. P. V. Ganesan, N. Luckashenak, M. Mendonca, and L. C. Eisenlohr.** 2015. Endogenous antigen processing drives the primary CD4(+) T cell response to influenza. Nature Medicine **21:**1216-+.
68. **Mimura, Y., Y. Mimura-Kimura, K. Doores, D. Golgher, B. G. Davis, R. A. Dwek, P. M. Rudd, and T. Elliott.** 2007. Folding of an MHC class II-restricted tumor antigen controls its antigenicity via MHC-guided processing. Proceedings of the National Academy of Sciences of the United States of America **104:**5983-5988.
69. **Mirano-Bascos, D., N. K. Steede, J. E. Robinson, and S. J. Landry.** 2010. Influence of Disulfide-Stabilized Structure on the Specificity of Helper T-Cell and Antibody Responses to HIV Envelope Glycoprotein gp120. Journal of Virology **84:**3303-3311.
70. **Mirano-Bascos, D., M. Tary-Lehmann, and S. J. Landry.** 2008. Antigen structure influences helper T-cell epitope dominance in the human immune response to HIV envelope glycoprotein gp120. European Journal of Immunology **38:**1231-1237.
71. **Modis, Y., S. Ogata, D. Clements, and S. C. Harrison.** 2003. A ligand-binding pocket in the dengue virus envelope glycoprotein. Proc Natl Acad Sci U S A **100:**6986-91.
72. **Modis, Y., S. Ogata, D. Clements, and S. C. Harrison.** 2005. Variable surface epitopes in the crystal structure of dengue virus type 3 envelope glycoprotein. J Virol **79:**1223-31.

73. **Monath, T. P.** 2008. Treatment of yellow fever. Antiviral Research **78:**116-124.
74. **Monath, T. P.** 2005. Yellow fever vaccine. Expert Review of Vaccines **4:**553-574.
75. **Monath, T. P., and A. D. T. Barrett.** 2003. Pathogenesis and pathophysiology of yellow fever. Flaviviruses: Pathogenesis and Immunity **60:**343-395.
76. **Monath, T. P., R. Nichols, W. T. Archambault, L. Moore, R. Marchesani, J. Tian, R. E. Shope, N. Thomas, R. Schrader, D. Furby, and P. Bedford.** 2002. Comparative safety and immunogenicity of two yellow fever 17D vaccines (ARILVAX and YF-VAX) in a phase III multicenter, double-blind clinical trial. Am J Trop Med Hyg **66:**533-41.
77. **Mortimer, P.** 2000. The use of yellow fever virus modified by in vitro cultivation for human immunization (Reprinted from J. Exp. Med. vol 65, pg 787-800, 1937). Reviews in Medical Virology **10:**3-13.
78. **Mukhopadhyay, S., R. J. Kuhn, and M. G. Rossmann.** 2005. A structural perspective of the flavivirus life cycle. Nat Rev Microbiol **3:**13-22.
79. **Nayak, J. L., K. A. Richards, F. A. Chaves, and A. J. Sant.** 2010. Analyses of the Specificity of CD4 T Cells During the Primary Immune Response to Influenza Virus Reveals Dramatic MHC-Linked Asymmetries in Reactivity to Individual Viral Proteins. Viral Immunology **23:**169-180.
80. **Neefjes, J., M. L. Jongsma, P. Paul, and O. Bakke.** 2011. Towards a systems understanding of MHC class I and MHC class II antigen presentation. Nat Rev Immunol **11:**823-36.
81. **Nguyen, H. N. P., N. K. Steede, J. E. Robinson, and S. J. Landry.** 2015. Conformational instability governed by disulfide bonds partitions the dominant from subdominant helper T-cell responses specific for HIV-1 envelope glycoprotein gp120. Vaccine **33:**2887-2896.
82. **Nielsen, M., and O. Lund.** 2009. NN-align. An artificial neural network-based alignment algorithm for MHC class II peptide binding prediction. BMC Bioinformatics **10:**296.
83. **Nielsen, M., O. Lund, S. Buus, and C. Lundegaard.** 2010. MHC class II epitope predictive algorithms. Immunology **130:**319-28.
84. **Nielsen, M., C. Lundegaard, T. Blicher, B. Peters, A. Sette, S. Justesen, S. Buus, and O. Lund.** 2008. Quantitative predictions of peptide binding to any HLA-DR molecule of known sequence: NetMHCIIpan. PLoS Comput Biol **4:**e1000107.
85. **Nielsen, M., C. Lundegaard, and O. Lund.** 2007. Prediction of MHC class II binding affinity using SMM-align, a novel stabilization matrix alignment method. BMC Bioinformatics **8:**238.
86. **Nybakken, G. E., C. A. Nelson, B. R. Chen, M. S. Diamond, and D. H. Fremont.** 2006. Crystal structure of the West Nile virus envelope glycoprotein. J Virol **80:**11467-74.
87. **Pei, J. M., B. H. Kim, M. Tang, and N. V. Grishin.** 2007. PROMALS web server for accurate multiple protein sequence alignments. Nucleic Acids Research **35:**W649-W652.
88. **Pfister, M., O. Kursteiner, H. Hilfiker, D. Favre, P. Durrer, A. Ennaji, J. L'Age-Stehr, A. Kaufhold, and C. Herzog.** 2005. Immunogenicity and safety of BERNA-YF compared with two other 17D yellow fever vaccines in a phase 3 clinical trial. American Journal of Tropical Medicine and Hygiene **72:**339-346.
89. **Pierson, T. C., and M. S. Diamond.** 2012. Degrees of maturity: the complex structure and biology of flaviviruses. Current Opinion in Virology **2:**168-175.
90. **Pierson, T. C., and M. S. Diamond.** 2013. Flaviviruses, p. 747-794. *In* D. M. Knipe, P. M. Howley, J. I. Cohen, D. E. Griffin, R. A. Lamb, M. A. Martin, V. R. Racaniello, and B. Roizman (ed.), Fields Virology, 6 ed. Lippincott. Williams & Wilkins., Philadelphia.
91. **Pierson, T. C., and M. S. Diamond.** 2008. Molecular mechanisms of antibody-mediated neutralisation of flavivirus infection. Expert Rev Mol Med **10:**e12.
92. **Poland, J. D., C. H. Calisher, T. P. Monath, W. G. Downs, and K. Murphy.** 1981. Persistence of Neutralizing Antibody 30-35 Years after Immunization with 17d Yellow-Fever Vaccine. Bulletin of the World Health Organization **59:**895-900.
93. **Pos, W., D. K. Sethi, and K. W. Wucherpfennig.** 2013. Mechanisms of peptide repertoire selection by HLA-DM. Trends in Immunology **34:**495-501.
94. **Rey, F. A., F. X. Heinz, C. Mandl, C. Kunz, and S. C. Harrison.** 1995. The envelope glycoprotein from tick-borne encephalitis virus at 2 A resolution. Nature **375:**291-8.

95. **Richards, K. A., F. A. Chaves, F. R. Krafcik, D. J. Topham, C. A. Lazarski, and A. J. Sant.** 2007. Direct ex vivo analyses of HLA-DR1 transgenic mice reveal an exceptionally broad pattern of immunodominance in the primary HLA-DR1-restricted CD4 T-cell response to influenza virus hemagglutinin. J Virol **81:**7608-19.
96. **Richter, M. K. S., J. M. D. Voorham, S. T. Pedraza, T. E. Hoornweg, D. P. I. van de Pol, I. A. Rodenhuis-Zybert, J. Wilschut, and J. M. Smit.** 2014. Immature Dengue Virus Is Infectious in Human Immature Dendritic Cells via Interaction with the Receptor Molecule DC-SIGN. Plos One **9**.
97. **Rivino, L., E. A. Kumaran, V. Jovanovic, K. Nadua, E. W. Teo, S. W. Pang, G. H. Teo, V. C. Gan, D. C. Lye, Y. S. Leo, B. J. Hanson, K. G. Smith, A. Bertoletti, D. M. Kemeny, and P. A. Macary.** 2013. Differential Targeting of Viral Components by CD4+ versus CD8+ T Lymphocytes in Dengue Virus Infection. J Virol **87:**2693-706.
98. **Roche, P. A., and K. Furuta.** 2015. The ins and outs of MHC class II-mediated antigen processing and presentation. Nature Reviews Immunology **15:**203-216.
99. **Rodenhuis-Zybert, I. A., H. M. van der Schaar, J. M. D. Voorham, H. van der Ende-Metselaar, H. Y. Lei, J. Wilschut, and J. M. Smit.** 2010. Immature Dengue Virus: A Veiled Pathogen? Plos Pathogens **6**.
100. **Roehrig, J. T., K. E. Volpe, J. Squires, A. R. Hunt, B. S. Davis, and G. J. Chang.** 2004. Contribution of disulfide bridging to epitope expression of the dengue type 2 virus envelope glycoprotein. J Virol **78:**2648-52.
101. **Rosenzweig, E. C., C. L. Wisseman, and R. W. Babione.** 1963. Immunological Studies with Group B Arthropod-Borne Viruses .4. Persistence of Yellow Fever Antibodies Following Vaccination with 17d Strain Yellow Fever Vaccine. American Journal of Tropical Medicine and Hygiene **12:**230-&.
102. **Russell, S. M., and F. Y. Liew.** 1979. T cells primed by influenza virion internal components can cooperate in the antibody response to haemagglutinin. Nature **280:**147-8.
103. **Sant, A. J., F. A. Chaves, S. A. Jenks, K. A. Richards, P. Menges, J. M. Weaver, and C. A. Lazarski.** 2005. The relationship between immunodominance, DM editing, and the kinetic stability of MHC class II : peptide complexes. Immunological Reviews **207:**261-278.
104. **Sant, A. J., F. A. Chaves, F. R. Krafcik, C. A. Lazarski, P. Menges, K. Richards, and J. M. Weaver.** 2007. Immunodominance in CD4 T-cell responses: implications for immune responses to influenza virus and for vaccine design. Expert Rev Vaccines **6:**357-68.
105. **Scherle, P. A., and W. Gerhard.** 1988. Differential ability of B cells specific for external vs. internal influenza virus proteins to respond to help from influenza virus-specific T-cell clones in vivo. Proc Natl Acad Sci U S A **85:**4446-50.
106. **Scherle, P. A., and W. Gerhard.** 1986. Functional analysis of influenza-specific helper T cell clones in vivo. T cells specific for internal viral proteins provide cognate help for B cell responses to hemagglutinin. J Exp Med **164:**1114-28.
107. **Schwaiger, J., J. H. Aberle, K. Stiasny, B. Knapp, W. Schreiner, I. Fae, G. Fischer, O. Scheinost, V. Chmelik, and F. X. Heinz.** 2014. Specificities of Human CD4(+) T Cell Responses to an Inactivated Flavivirus Vaccine and Infection: Correlation with Structure and Epitope Prediction. Journal of Virology **88:**7828-7842.
108. **Sercarz, E. E., and E. Maverakis.** 2003. MHC-guided processing: Binding of large antigen fragments. Nature Reviews Immunology **3:**621-629.
109. **Sette, A., L. Adorini, S. M. Colon, S. Buus, and H. M. Grey.** 1989. Capacity of intact proteins to bind to MHC class II molecules. J Immunol **143:**1265-7.
110. **Sidney, J., E. Assarsson, C. Moore, S. Ngo, C. Pinilla, A. Sette, and B. Peters.** 2008. Quantitative peptide binding motifs for 19 human and mouse MHC class I molecules derived using positional scanning combinatorial peptide libraries. Immunome Res **4:**2.
111. **Simmonds, P., P. Becher, M. S. Collett, E. A. Gould, F. X. Heinz, G. Meyers, T. Monath, A. Pletnev, C. M. Rice, K. Stiasny, H. J. Thiel, A. Weiner, and J. Bukh.** 2011. Family Flaviviridae, p. 1003-1020. *In* A. M. Q. King, E. Lefkowitz, M. J. Adams, and E. B. Carstens (ed.), Virus

Taxonomy. IXth Report of the International Committee on Taxonomy of Viruses. Elsevier Academic Press, San Diego.
112. **Sitati, E. M., and M. S. Diamond.** 2006. CD4+ T-cell responses are required for clearance of West Nile virus from the central nervous system. J Virol **80:**12060-9.
113. **Staples, J. E., J. A. Bocchini, L. Rubin, and M. Fischer.** 2015. Yellow Fever Vaccine Booster Doses: Recommendations of the Advisory Committee on Immunization Practices, 2015. Mmwr-Morbidity and Mortality Weekly Report **64:**647-650.
114. **Stern, L. J., and L. Santambrogio.** 2016. The melting pot of the MHC II peptidome. Curr Opin Immunol **40:**70-77.
115. **Stiasny, K., R. Fritz, K. Pangerl, and F. X. Heinz.** 2011. Molecular mechanisms of flavivirus membrane fusion. Amino Acids **41:**1159-63.
116. **Stiasny, K., and F. X. Heinz.** 2006. Flavivirus membrane fusion. J Gen Virol **87:**2755-66.
117. **Stiasny, K., H. Holzmann, and F. X. Heinz.** 2009. Characteristics of antibody responses in tick-borne encephalitis vaccination breakthroughs. Vaccine **27:**7021-7026.
118. **Stiasny, K., S. Kiermayr, A. Bernhart, and F. X. Heinz.** 2013. The Membrane-Proximal "Stem" Region Increases the Stability of the Flavivirus E Protein Postfusion Trimer and Modulates Its Structure. Journal of Virology **87:**9933-9938.
119. **Stiasny, K., S. Kiermayr, H. Holzmann, and F. X. Heinz.** 2006. Cryptic properties of a cluster of dominant flavivirus cross-reactive antigenic sites. J Virol **80:**9557-68.
120. **Sturniolo, T., E. Bono, J. Ding, L. Raddrizzani, O. Tuereci, U. Sahin, M. Braxenthaler, F. Gallazzi, M. P. Protti, F. Sinigaglia, and J. Hammer.** 1999. Generation of tissue-specific and promiscuous HLA ligand databases using DNA microarrays and virtual HLA class II matrices. Nat Biotechnol **17:**555-61.
121. **Su, L. F., B. A. Kidd, A. Han, J. J. Kotzin, and M. M. Davis.** 2013. Virus-Specific CD4(+) Memory-Phenotype T Cells Are Abundant in Unexposed Adults. Immunity **38:**373-383.
122. **Surman, S., T. D. Lockey, K. S. Slobod, B. Jones, J. M. Riberdy, S. W. White, P. C. Doherty, and J. L. Hurwitz.** 2001. Localization of CD4+ T cell epitope hotspots to exposed strands of HIV envelope glycoprotein suggests structural influences on antigen processing. Proc Natl Acad Sci U S A **98:**4587-92.
123. **Tenzer, S., E. Wee, A. Burgevin, G. Stewart-Jones, L. Friis, K. Lamberth, C. H. Chang, M. Harndahl, M. Weimershaus, J. Gerstoft, N. Akkad, P. Klenerman, L. Fugger, E. Y. Jones, A. J. McMichael, S. Buus, H. Schild, P. van Endert, and A. K. Iversen.** 2009. Antigen processing influences HIV-specific cytotoxic T lymphocyte immunodominance. Nat Immunol **10:**636-46.
124. **van der Most, R. G., L. E. Harrington, V. Giuggio, P. L. Mahar, and R. Ahmed.** 2002. Yellow fever virus 17D envelope and NS3 proteins are major targets of the antiviral T cell response in mice. Virology **296:**117-124.
125. **Vinuesa, C. G., S. G. Tangye, B. Moser, and C. R. Mackay.** 2005. Follicular B helper T cells in antibody responses and autoimmunity. Nat Rev Immunol **5:**853-65.
126. **Vratskikh, O., K. Stiasny, J. Zlatkovic, G. Tsouchnikas, J. Jarmer, U. Karrer, M. Roggendorf, H. Roggendorf, R. Allwinn, and F. X. Heinz.** 2013. Dissection of Antibody Specificities Induced by Yellow Fever Vaccination. Plos Pathogens **9**.
127. **Wang, P., J. Sidney, C. Dow, B. Mothe, A. Sette, and B. Peters.** 2008. A systematic assessment of MHC class II peptide binding predictions and evaluation of a consensus approach. PLoS Comput Biol **4:**e1000048.
128. **Wang, P., J. Sidney, Y. Kim, A. Sette, O. Lund, M. Nielsen, and B. Peters.** 2010. Peptide binding predictions for HLA DR, DP and DQ molecules. BMC Bioinformatics **11:**568.
129. **Weaver, J. M., C. A. Lazarski, K. A. Richards, F. A. Chaves, S. A. Jenks, P. R. Menges, and A. J. Sant.** 2008. Immunodominance of CD4 T cells to foreign antigens is peptide intrinsic and independent of molecular context: Implications for vaccine design. Journal of Immunology **181:**3039-3048.
130. **Wen, J. S., L. F. Jiang, J. M. Zhou, H. J. Yan, and D. Y. Fang.** 2008. Computational prediction and identification of dengue virus-specific CD4(+) T-cell epitopes. Virus Res **132:**42-8.

131. **WHO.** 2016. Yellow fever fact sheet. http://www.who.int/mediacentre/factsheets/fs100/en/.
132. **WHO.** 2016. Zika virus fact sheet. http://www.who.int/mediacentre/factsheets/zika/en/.
133. **Yi, W., N. P. Seth, T. Martillotti, K. W. Wucherpfennig, D. B. Sant'Angelo, and L. K. Denzin.** 2010. Targeted regulation of self-peptide presentation prevents type I diabetes in mice without disrupting general immunocompetence. Journal of Clinical Investigation **120:**1324-1336.
134. **Zhang, W., P. R. Chipman, J. Corver, P. R. Johnson, Y. Zhang, S. Mukhopadhyay, T. S. Baker, J. H. Strauss, M. G. Rossmann, and R. J. Kuhn.** 2003. Visualization of membrane protein domains by cryo-electron microscopy of dengue virus. Nat Struct Biol **10:**907-12.